

Conformal prediction for dynamic time-series

Chen Xu

CXU310@GATECH.EDU

*Industrial and Systems Engineering
Georgia Institute of Technology
Atlanta, GA 30332, USA*

Yao Xie

YAO.XIE@ISYE.GATECH.EDU

*Industrial and Systems Engineering
Georgia Institute of Technology
Atlanta, GA 30332, USA*

Abstract

We develop a general framework constructing distribution-free prediction intervals for dynamic time series. We show that our intervals asymptotically attain valid conditional and marginal coverages for a broad class of predictions functions and time series. We also show that our interval width converges to that of the oracle prediction interval asymptotically. Moreover, we introduce a computationally efficient algorithm called **EnbPI** that wraps around ensemble predictors, which is closely related to conformal prediction (CP) but does not require data exchangeability. **EnbPI** avoids data-splitting and is computationally efficient by avoiding retraining and thus scalable to sequentially producing prediction intervals. We perform extensive simulation and real-data analyses to demonstrate its effectiveness compared with existing methods.

Keywords: time-series predictive inference, conformal prediction, asymptotic guarantee, network inference with missing data, anomaly detection

1. Introduction

Modern applications, including energy and supply chains (Díaz-González et al., 2012; Cochran et al., 2015), require sequential prediction with uncertainty quantification for dynamic time-series observations with highly complex spatio-temporal dependency. Time-series are dynamic as they may contain unobserved errors that are non-stationary. It is typical to construct prediction intervals for uncertainty quantification, a fundamental task in statistics and machine learning.

Constructing accurate prediction intervals for dynamic time series is highly challenging. For instance, it is crucial to accurately predict energy levels from wind farms and solar roof panels using historical data and construct prediction intervals for statistical inference to incorporate renewable energy into existing power systems. However, as outlined in the National Renewable Energy Lab report (Cochran et al., 2015), solar and wind power generation data are non-stationary, with significant stochastic variations and spatial-temporal correlations among regions. Meanwhile, complex prediction functions such as random forest (Breiman, 2001) and deep neural networks (Lathuilière et al., 2019) are often used for prediction; unlike classical linear regression models, such prediction algorithms do not have

explicit forms of prediction intervals. In practice, to achieve more powerful prediction performance, ensemble methods (Breiman, 1996) are commonly used to combine multiple prediction algorithms, further increasing model complexity. Thus, efficiently constructing prediction intervals (that is, beyond a point prediction) for dynamic time series using general complex prediction methods remains unanswered.

1.1 Contributions

In this paper, we develop distribution-free prediction intervals for dynamic time-series data with a coverage guarantee, inspired by the recent works on conformal prediction. In particular, our method **EnbPI** can provide prediction intervals for ensemble prediction algorithms. We summarize the main contributions as follows.

- We present a general framework for constructing (possibly) asymmetrical prediction intervals for time series and theoretically show asymptotically valid conditional and marginal coverage under mild assumptions on the dependency of stochastic errors and the quality of estimation. Intervals also converge in width to the oracle prediction interval.
- We present **EnbPI**, a robust and computationally efficient algorithm around ensemble estimators. It avoids expensive model retraining during prediction and requires no data splitting due to a carefully constructed bootstrap procedure and thus works well for small-sample problems. Moreover, it is versatile and can apply in various practical settings such as anomaly detection and network prediction.
- We study the performance of **EnbPI** on simulated and real data examples using extensive numerical experiments. We show that **EnbPI** can maintain a target coverage when competing methods fail to do so and yield shorter intervals for highly dynamic time series. Moreover, we demonstrate using examples that **EnbPI** is robust to missing data.

The rest of this paper is organized as follows. Section 2 sets up the problem setup and introduces the oracle prediction interval, which motivates our proposed method. Section 3 presents asymptotic guarantees for interval coverage and width and highlights the generality of such guarantees. Section 4 presents **EnbPI**. Section 5 contains numerical examples with simulated and real data that compare **EnbPI** with competing methods to demonstrate its good performance in various scenarios. Section 6 extends the use of **EnbPI** when a change point exist. Section 7 concludes the paper with discussions. Appendix A contains all the proofs. Appendix B illustrates additional experimental results. Code for our method can be found at <https://github.com/hamrel-cxu/EnbPI>.

1.2 Literature review

Conformal Prediction (CP) is becoming increasingly used for constructing distribution-free prediction intervals. Formally introduced in (Shafer and Vovk, 2008), the CP method assigns “conformity scores”¹ to training and test data. Prediction intervals for test data are obtained by inverting hypothesis tests with these scores. It is shown that under exchangeability in data, this procedure generates exactly valid marginal coverage of the test point. Many

1. In this paper, conformity scores are defined as prediction residuals.

existing works such as (Papadopoulos et al., 2007; Romano et al., 2019; Gupta et al., 2019; Barber et al., 2019b; Kivaranovic et al., 2020; Izbicki et al., 2020; Dunn et al., 2020; Gupta et al., 2021; Fisch et al., 2021a,b) have utilized this idea. Comprehensive surveys and tutorials can be found in (Shafer and Vovk, 2008; Zeni et al., 2020). Although no assumption other than data exchangeability is required for marginally exact coverage, the exchangeability assumption is hardly reasonable for time series. Recently, adapting CP methods beyond exchangeable data has also been gaining significant interests. The work by Tibshirani et al. (2019) uses weighted conformal prediction intervals when the test data distribution is proportional to the training distribution. Another work by Cauchois et al. (2020) provides a coverage guarantee when the shifted test distribution lies in an f -divergence ball around the training distribution. However, both works still assume *i.i.d.* or exchangeable training data, making them not directly applicable for time-series. Moreover, Gibbs and Candès (2021) provides approximately valid coverage on sequential data when marginal distributions of test data have small shifts by re-weighting the coverage level $(1 - \alpha)$. However, whether the method can be applied to data with general dependency remains unclear even under no distribution shift. On the other hand, recent works by Chernozhukov et al. (2018, 2020) study conformal inference for time series data; their assumptions and proof techniques motivate our theoretical analyses. Here we refine the proof techniques to improve the convergence rates and extend results under different assumptions. We further analyze the widths of our confidence intervals relative to the oracle. Moreover, compared with our proposed algorithm **EnbPI**, the existing methods in Chernozhukov et al. (2018, 2020) rely on data-splitting and may be computationally intensive for ensemble methods.

Finally, we remark that our assumptions and proof techniques avoid data exchangeability and differ significantly from existing CP works. Most CP methods ensure finite-sample marginal coverage and distribution-free conditional coverage is impossible at finite sample size (Barber et al., 2019a), while we can achieve asymptotic conditional coverage. Our work is titled “conformal prediction” mostly because **EnbPI** is inspired by the Jackknife+-after-bootstrap (J+aB) (Kim et al., 2020), which is an efficient CP-based algorithm developed for ensemble methods assuming data exchangeability; here, we extend the idea to time series without assuming exchangeability while providing conditional coverage guarantee.

We want to remark that there are many non-CP prediction interval methods in the classic time-series literature (Brockwell et al., 1991). Traditional time-series methods such as ARIMA(p, d, q) (Durbin and Koopman, 2012), exponential smoothing (Hyndman et al., 2008), dynamic factor models (Bańbura and Modugno, 2014), and so on, have been widely successful. We will compare **EnbPI** with some of these methods in experiments.

2. Problem setup

Given an unknown model $f : \mathbb{R}^d \rightarrow \mathbb{R}$, where d is the dimension of the feature vector, we observe data (x_t, y_t) generated according to the following model

$$Y_t = f(X_t) + \epsilon_t, \quad t = 1, 2, \dots \quad (1)$$

where ϵ_t is distributed following a continuous cumulative distribution function (CDF) F_t . Note that we do not need ϵ_t to be independent and F_t needs not be the same across all t . Features X_t can contain exogenous time-series sequences that predict Y_t and/or the history

of Y_t . We assume that the first T samples $\{(x_t, y_t)\}_{t=1}^T$ are training data or initial state of the random process that are observable. Above, upper case X_t, Y_t denote random variables and lower case x_t, y_t denote data.

Our goal is to construct a sequence of prediction intervals as narrow as possible with a certain coverage guarantee. Given a user-specified prediction algorithm, using T training samples, we obtain a trained model represented by \hat{f} . Then we construct $s \geq 1$ prediction intervals $\{\hat{C}_{T+i}^\alpha\}_{i=1}^s$ for $\{Y_{T+i}\}_{i=1}^s$, where α is the *significance level*, and the *batch size* s is a pre-specified parameter for how many steps we want to look ahead. Once new samples $\{(x_{T+i}, y_{T+i})\}_{i=1}^s$ become available, we deploy the pre-trained \hat{f} on new samples and use the most recent T samples to produce prediction intervals for $Y_j, j = T + s + 1$ onward without re-training the model on new data.

The meaning of significance level α is as follows. We consider two types of coverage guarantees. The *conditional* coverage guarantee ensures that each prediction interval $\hat{C}_t^\alpha, t > T$ satisfies:

$$P(Y_t \in \hat{C}_t^\alpha | X_t = x_t) \geq 1 - \alpha. \quad (2)$$

The second type is the *marginal* coverage guarantee:

$$P(Y_t \in \hat{C}_t^\alpha) \geq 1 - \alpha. \quad (3)$$

Note that (2) is much stronger than (3), which is satisfied whenever data are exchangeable (Papadopoulos et al., 2007). For instance, suppose a doctor reports a prediction interval for one patient's blood pressure. An interval satisfying (3) averages over all patients in different age groups, but may not satisfy (2) for the current patient precisely. In fact, satisfying (2), even for exchangeable data, is impossible without further assumptions (Barber et al., 2019a). In general, it is challenging to ensure either (2) or (3) under complex data dependency without distributional assumptions. Despite such difficulty, we present an algorithm in Section 4, referred to as **EnbPI**, which can asymptotically satisfy the conditional coverage (2) under certain assumptions on the error process $\{\epsilon_t\}_{t \geq 1}$ and \hat{f} , and then the marginal coverage (3) follows. From now on, we call a prediction interval conditionally or marginally *valid* if it achieves (2) or (3), respectively.

2.1 Oracle prediction interval

To motivate the construction of \hat{C}_t^α , we first consider the *oracle* prediction interval C_t^α , which contains Y_t with an exact conditional coverage at $1 - \alpha$ and is the shortest among all possible conditionally valid prediction intervals. The oracle prediction assumes perfect knowledge of f and F_t in (1). Denote $F_{t,Y}$ as the CDF of Y_t conditioning on $X_t = x_t$, then we have

$$F_{t,Y}(y) = \mathbb{P}(Y_t \leq y | X_t = x_t) = \mathbb{P}(\epsilon_t \leq y - f(x_t)) = F_t(y - f(x_t)).$$

For any $\beta \in [0, \alpha]$, we also know that

$$\mathbb{P}(Y_t \in [F_{t,Y}^{-1}(\beta), F_{t,Y}^{-1}(1 - \alpha + \beta)] | X_t = x_t) = 1 - \alpha,$$

where $F_{t,Y}^{-1}(\beta) := \inf\{y : F_{t,Y}(y) \geq \beta\}$. Assume $F_{t,Y}^{-1}(\alpha)$ is attained for each $\alpha \in [0, 1]$, and let $y_\beta = F_{t,Y}^{-1}(\beta)$. Clearly,

$$y_\beta = f(x_t) + F_t^{-1}(\beta),$$

which allows us to find C_t^α – the oracle prediction interval with the narrowest width:

$$\begin{aligned} C_t^\alpha &= [f(x_t) + F_t^{-1}(\beta^*), f(x_t) + F_t^{-1}(1 - \alpha + \beta^*)], \\ \beta^* &:= \arg \min_{\beta \in [0, \alpha]} (F_t^{-1}(1 - \alpha + \beta) - F_t^{-1}(\beta)). \end{aligned} \quad (4)$$

Thus, if we can approximate unknown $f(x_t)$, $F_t^{-1}(x)$, $x \in [0, 1]$, and β^* reasonably well, we can construct prediction intervals \hat{C}_t^α that are close to the oracle C_t^α .

2.2 Proposed prediction interval

We now construct \hat{C}_t^α based on ideas above. Recall that the first T data $\{(x_t, y_t)\}_{t=1}^T$ are observable. Denote \hat{f}_{-i} as the i -th “leave-one-out” (LOO) estimator of f , which is not trained on the i -th datum (x_i, y_i) and may include the remaining $T - 1$ points. Then,

$$\begin{aligned} \hat{C}_t^\alpha &:= [\hat{f}_{-t}(x_t) + \hat{\beta} \text{ quantile of } \{\hat{\epsilon}_i\}_{i=t-1}^{t-T}, \\ &\quad \hat{f}_{-t}(x_t) + (1 - \alpha + \hat{\beta}) \text{ quantile of } \{\hat{\epsilon}_i\}_{i=t-1}^{t-T}], \end{aligned} \quad (5)$$

where the LOO prediction residual $\hat{\epsilon}_i$ and the corresponding $\hat{\beta}$ are defined as

$$\begin{aligned} \hat{\epsilon}_i &:= y_i - \hat{f}_{-i}(x_i), \\ \hat{\beta} &:= \arg \min_{\beta \in [0, \alpha]} \left((1 - \alpha + \beta) \text{ quantile of } \{\hat{\epsilon}_i\}_{i=t-1}^{t-T} - \beta \text{ quantile of } \{\hat{\epsilon}_i\}_{i=t-1}^{t-T} \right). \end{aligned}$$

Thus, the interval centers at the point prediction $\hat{f}_{-t}(x_t)$ and its width is the difference between the $(1 - \alpha + \hat{\beta})$ and $\hat{\beta}$ quantiles over the past T residuals.

Note that we have to split the training data into two parts: one part is used to estimate f , and the second part is used to obtain prediction residuals for the prediction interval. There is a trade-off. On the one hand, we desire the estimator \hat{f} to be trained on as much data as possible. On the other hand, the quantile of prediction residuals should well approximate the tails of F_t^{-1} . These two objectives contradict each other. If we train \hat{f} on all training data, then we overfit; if we train on a subset of training data and obtain prediction residuals on the rest (Papadopoulos et al., 2007), the approximation \hat{f} to f is poorer. The LOO estimator is known to achieve a good trade-off in this regard. The LOO idea is related to the Jackknife+ procedure (Barber et al., 2019b), but it is known to be costly due to the retraining of the model. To address this issue, we will develop a computationally efficient method called **EnbPI** in Section 4, which constructs the LOO estimators as *ensemble* estimators of pre-trained models.

3. Theoretical analysis

We first present theoretical results for asymptotic conditional validity, upon which marginal validity follows. We then prove that proposed prediction intervals converge to oracle ones. We lastly provide several important remarks regarding the applicability of the guarantees. In particular, the results are general for methods beyond **EnbPI** (for example, split conformal (Papadopoulos et al., 2007)), yet with noticeable caveats in Remark 3 regarding issues of

data splitting. We will also discuss how the assumptions are reasonable and can be satisfied. All proofs of Lemmas, Theorems, and Corollaries can be found in Appendix A.

Without loss of generality and for notation simplicity, we only show guarantees when $t = T + 1$, the one-step-ahead prediction. We will explain how guarantees naturally extend to all prediction intervals from $t = T + 2$ onward in Remark 4. In particular, our proof removes the assumptions on data exchangeability by replacing them with general and verifiable assumptions on the error process and estimation quality.

3.1 Coverage guarantees

Following the notation in Section 2.1, we first define the empirical p -value at $T + 1$:

$$\hat{p}_{T+1} := \frac{1}{T} \sum_{i=1}^T \mathbf{1}\{\hat{\epsilon}_i \leq \hat{\epsilon}_{T+1}\}.$$

As a result, we see the following equivalence between events:

$$\begin{aligned} & Y_{T+1} \in \hat{C}_{T+1}^\alpha | X_{T+1} = x_{T+1} \\ \iff & \hat{\epsilon}_{T+1} \in [\hat{\beta} \text{ quantile of } \{\hat{\epsilon}_i\}_{i=T}^1, (1 - \alpha + \hat{\beta}) \text{ quantile of } \{\hat{\epsilon}_i\}_{i=T}^1] \Big| X_{T+1} = x_{T+1} \\ \iff & \hat{\beta} \leq \hat{p}_{T+1} \leq 1 - \alpha + \hat{\beta} \end{aligned}$$

where $A|B$ means that the event A conditions on event B . Therefore, our method covers Y_{T+1} given $X_{T+1} = x_{T+1}$ with probability $1 - \alpha$, hence, being conditionally valid if the distribution of \hat{p}_{T+1} is uniform. More precisely, we aim to ensure that $|\mathbb{P}(\beta \leq \hat{p}_{T+1} \leq 1 - \alpha + \beta) - (1 - \alpha)|$ is small for any $\beta \in [0, \alpha]$.

Due to the fact that $F_{T+1}(\epsilon_{T+1}) \sim \text{Unif}[0, 1]$ (Dodge, 2006), $\mathbb{P}(\beta \leq F_{T+1}(\epsilon_{T+1}) \leq 1 - \alpha + \beta) = 1 - \alpha$. Inspired by this observation, define

$$\hat{F}_{T+1}(x) := \frac{1}{T} \sum_{i=1}^T \mathbf{1}\{\hat{\epsilon}_i \leq x\},$$

which is the empirical CDF of $\hat{\epsilon}_{T+1}$ and we have $\hat{p}_{T+1} = \hat{F}_{T+1}(\hat{\epsilon}_{T+1})$. As a consequence:

$$\begin{aligned} & |\mathbb{P}(\beta \leq \hat{p}_{T+1} \leq 1 - \alpha + \beta) - (1 - \alpha)| \\ &= |\mathbb{P}(\beta \leq \hat{F}_{T+1}(\hat{\epsilon}_{T+1}) \leq 1 - \alpha + \beta) - \mathbb{P}(\beta \leq F_{T+1}(\epsilon_{T+1}) \leq 1 - \alpha + \beta)|. \end{aligned}$$

Thus, we can prove the conditional coverage if $\hat{F}_{T+1}(\hat{\epsilon}_{T+1})$ is close in distribution to $F_{T+1}(\epsilon_{T+1})$. Notice the following coupling between $\hat{\epsilon}_{T+1}$ and ϵ_{T+1} under model (1) when $X_{T+1} = x_{T+1}$:

$$\hat{\epsilon}_{T+1} = \epsilon_{T+1} + (f(x_{T+1}) - \hat{f}_{-(T+1)}(x_{T+1})).$$

Therefore, the pointwise function estimation error $f(x_{T+1}) - \hat{f}_{-(T+1)}(x_{T+1})$ should be small in order for $\hat{\epsilon}_{T+1}$ to be a good estimate for ϵ_{T+1} . We will impose this condition when proving asymptotic convergence in interval width.

For the analyses, we now introduce another empirical CDF using unknown errors $\epsilon_i, i \geq 1$, which we denote as \tilde{F}_{T+1} :

$$\tilde{F}_{T+1}(x) := \frac{1}{T} \sum_{i=1}^T \mathbf{1}\{\epsilon_i \leq x\}.$$

Note that $\hat{F}_{T+1}(\hat{\epsilon}_{T+1})$ is close in distribution to $\tilde{F}_{T+1}(\epsilon_{T+1})$ under the same pointwise estimation assumption of f by \hat{f} . Meanwhile, the convergence of $\tilde{F}_{T+1}(x)$ to $F_{T+1}(x)$ is a well-understood question in probability, which addresses the rate of convergence of an empirical distribution to the actual CDF. There are many results assuming that the unknown errors $\{\epsilon_t\}_{t=1}^{T+1}$ have certain dependency structure.

Building on notations and ideas above, we now state the precise assumptions with discussions and present the following results: we first bound the worst deviation between $\tilde{F}_{T+1}(x)$ and $F_{T+1}(x)$ in Lemma 1. We then bound that between $\hat{F}_{T+1}(x)$ and $\tilde{F}_{T+1}(x)$ in Lemma 2. These lemmas are essential to proving our main theoretical results in Theorem 1, which has several useful corollaries under slightly modified assumptions on error dependencies.

Assumption 1 (Errors are short-term i.i.d.). *Assume $\{\epsilon_t\}_{t=1}^{T+1}$ are independent and identically distributed (i.i.d.) according to a common CDF F_{T+1} , which is Lipschitz continuous with constant $L_{T+1} > 0$.*

Lemma 1. *Suppose Assumption 1 holds. Then, for any training size T , there is an event A_T in the probability space of $\{\epsilon_t\}_{t=1}^T$, such that conditioning on A_T ,*

$$\sup_x |\tilde{F}_{T+1}(x) - F_{T+1}(x)| \leq \sqrt{\log(16T)/T}.$$

Moreover,

$$P(A_T^C) \leq \sqrt{\log(16T)/T}.$$

Discussion on Assumption 1. We call it the short-term i.i.d. assumption because we only require the past $T + 1$ errors to be independent. It is a mild assumption on the original process $\{(X_t, Y_t)\}_{t \geq 1}$, because the process can exhibit arbitrary dependence and be highly non-stationary, but still have i.i.d. errors. Common time-series with i.i.d. errors include non-stationary random walks and ARIMA(p, d, q) models. Meanwhile, we can empirically examine whether Assumption 1 holds by using the LOO residuals as surrogates. The procedure is similar to examining the autocorrelation function after fitting an ARIMA model on time-series data.

Assumption 2 (Estimation quality). *There exists a real sequence $\{\delta_T\}_{T \geq 1}$ that converges to zero such that*

$$\frac{1}{T} \sum_{t=1}^T (\hat{f}_{-t}(x_t) - f(x_t))^2 \leq \delta_T^2.$$

Lemma 2. *Assume Assumption 1 and 2 hold. Define $C := L_{T+1} + 1$ whereby*

$$\sup_x |\hat{F}_{T+1}(x) - \tilde{F}_{T+1}(x)| \leq C\delta_T^{2/3} + 2 \sup_x |\tilde{F}_{T+1}(x) - F_{T+1}(x)|.$$

Discussion on Assumption 2. Firstly, one needs to avoid data overfitting, which leads to $\hat{f}_{-t}(x_t) \approx y_t$ so that we have $\sum_{t=1}^T (\hat{f}_{-t}(x_t) - f(x_t))^2 \approx \sum_{t=1}^T \epsilon_t^2$. If $\sum_{t=1}^T \epsilon_t^2 \in \Omega(T)$, the condition is never satisfied. Using LOO estimators can effectively alleviate the overfitting issue. Secondly, so long as estimators satisfies Assumption 2, the theoretical guarantee holds; we will build LOO ensemble predictors as they tend to further reduce function approximation errors required by the assumption. Lastly, the famous *No Free Lunch Theorem* (Wolpert and Macready, 1997) requires assumptions on the unknown f for good function approximation. We can find δ_T for two classes of f and the corresponding \mathcal{A} :

(Example 1) If f is sufficiently smooth, $\delta_T = o_P(T^{-1/4})$ for general neural networks sieve estimators (see Chen and White, 1999, Corollary 3.2).

(Example 2) If f is a sparse high-dimensional linear model, $\delta_T = o_P(T^{-1/2})$ for the Lasso estimator and Dantzig selector. (see Bickel et al., 2009, Equation 7.7).

In general, one needs to analyze the convergence rate of estimators \hat{f} to the unknown true f . This task is different from analyzing the Mean Squared Error (MSE) of ensemble estimators (Breiman, 1996) and likely requires case-by-case analyses. The task is even harder for ensemble estimators; the answers will belong to future work.

Remark 1 (When Assumption 2 fails). *In reality, there may be change points that alter the underlying f (Xie et al., 2021), whereby conditioning on $X_t = x_t$, pointwise approximation differences $\hat{f}_{-t}(x_t) - f(x_t), t \geq T$ become large if we use pre-trained estimators. If no action is taken, coverage can drop significantly because pre-changed residuals are used to calibrate widths of post-change prediction intervals. Besides refitting estimators, we can also adjust widths of prediction intervals by leveraging newly revealed samples, which will be explained as a crucial step of **EnbPI**. Section 6 uses **EnbPI** under the presence of a change point during prediction.*

Our main theoretical result is the following Theorem 1, which establishes the asymptotic conditional coverage as a consequence of Lemmas 1 and 2.

Theorem 1 (Asymptotic conditional coverage; errors are short-term i.i.d.). *Suppose Assumption 1 and 2 hold. Define $C := L_{T+1} + 1$. For any training size T , $\alpha \in (0, 1)$, and $\beta \in [0, \alpha]$, we have:*

$$|\mathbb{P}(Y_{T+1} \in \hat{C}_{T+1}^\alpha | X_{T+1} = x_{T+1}) - (1 - \alpha)| \leq 24\sqrt{\log(16T)/T} + 4C\delta_T^{2/3}.$$

We note that the right-hand side $\delta_T^{2/3}$ rate depends on the quality of function approximation and can only be faster under stricter requirements. On the other hand, the right-hand side $\sqrt{\log(16T)/T}$ rate is proved by analyzing how quickly the empirical CDF \tilde{F}_{T+1} converges to the actual CDF F_{T+1} . In particular, the crux is to provide similar versions of Lemma 1 by finding appropriate sequences s_T and $g(s_T)$, both of which converge to zero, such that

$$\mathbb{P}(\sup_x |\tilde{F}_{T+1}(x) - F_{T+1}(x)| > s_T) \leq g(s_T).$$

The optimal rate of decay reduces to finding s_T such that $s_T = g(s_T)$. Then, we can define A_T on which $\sup_x |\tilde{F}_{T+1}(x) - F_{T+1}(x)| \leq s_T$ and its complement A_T^C also happens

with probability no larger than s_T . As a result, we can find decay rates different from $\sqrt{\log(16T)/T}$ under increasing more relaxed assumptions on $\{\epsilon_t\}_{t=1}^{T+1}$, while still assuming a common CDF F_{T+1} with Lipschitz constant $L_{T+1} > 0$ for the past $T + 1$ errors. We summarize two possible results in Corollaries 1 and 2; certain technical assumptions, precise statements, and definitions are presented in the appendix.

Corollary 1 (Asymptotic conditional coverage; errors follow linear processes). *Suppose Assumption 2 holds and $\{\epsilon_t\}_{t=1}^{T+1}$ satisfy $\epsilon_t = \sum_{j=1}^{\infty} \delta_j z_{t-j}$, with regularity conditions on δ_j and z_{t-j} . Define $C = L_{T+1} + 1$. There exists a constant C_1 so that for any training size T , $\alpha \in (0, 1)$, and $\beta \in [0, \alpha]$, we have:*

$$|\mathbb{P}(Y_{T+1} \in \hat{C}_{T+1}^\alpha | X_{T+1} = x_{T+1}) - (1 - \alpha)| \leq 24C_1 \log T / \sqrt{T} + 4C\delta_T^{2/3}.$$

Define the strong mixing coefficient between two σ -fields \mathcal{A} and \mathcal{B} , which measures the dependence between them:

$$\alpha(\mathcal{A}, \mathcal{B}) = 2 \sup\{|\mathbb{P}(A \cap B) - \mathbb{P}(A)\mathbb{P}(B)| : (A, B) \in \mathcal{A} \times \mathcal{B}\}.$$

This definition is equivalent to that in (Rosenblatt, 1956) up to a multiplicative factor of 2. For the sequence $\{\epsilon_t\}_{t \geq 1}$, let $\mathcal{A}_k := \sigma(\epsilon_t : t \leq k)$ and $\mathcal{B}_l := \sigma(\epsilon_t : t \geq l)$. The coefficients $\{\alpha_n\}_{n \geq 1}$ are defined as

$$\alpha_0 = 1/2 \text{ and } \alpha_n = \sup_{k \in \mathbb{N}} \alpha(\mathcal{A}_k, \mathcal{B}_{k+n}) \text{ for any } n > 0.$$

The sequence is said to be *strongly mixing* if $\lim_{n \rightarrow \infty} \alpha_n = 0$.

Corollary 2 (Asymptotic conditional coverage; errors are strongly mixing). *Suppose Assumption 2 holds and $\{\epsilon_t\}_{t=1}^{T+1}$ are stationary and strongly mixing, where mixing coefficients are summable with $0 < \sum_{k \geq 0} \alpha_k < M$. Define $C = L_{T+1} + 1, C_1 = (M/2)^{1/3}$. For any training size T , $\alpha \in (0, 1)$, and $\beta \in [0, \alpha]$, we have:*

$$|\mathbb{P}(Y_{T+1} \in \hat{C}_{T+1}^\alpha | X_{T+1} = x_{T+1}) - (1 - \alpha)| \leq 24C_1 (\log T)^{2/3} / T^{1/3} + 4C\delta_T^{2/3}.$$

Lastly, the following asymptotic marginal validity guarantee holds as a consequence of earlier results by the tower law property (proof omitted):

Theorem 2 (Asymptotic marginal coverage). *Suppose Assumption 1 and 2 hold. Define $C := L_{T+1} + 1$. For any training size T , $\alpha \in (0, 1)$, and $\beta \in [0, \alpha]$, we have:*

$$|\mathbb{P}(Y_{T+1} \in \hat{C}_{T+1}^\alpha) - (1 - \alpha)| \leq 24\sqrt{\log(16T)/T} + 4C\delta_T^{2/3}.$$

Moreover, the right-hand side decay rate is

- $\mathcal{O}(\log T / \sqrt{T} + \delta_T^{2/3})$ if $\{\epsilon_t\}$ follow a linear process as in Corollary 1.
- $\mathcal{O}((\log T)^{2/3} / T^{1/3} + \delta_T^{2/3})$ if $\{\epsilon_t\}$ are strongly mixing with summable mixing coefficients as in Corollary 2.

We finally make several comments for Theorem 1, 2, and the two corollaries: (1) To build prediction intervals that have at least $1 - \alpha$ coverage, one needs to incorporate the upper bounds above into the prediction interval construction. We will not do so in **EnbPI**, as we aim to design a general wrapper that can be applied to most regression models \mathcal{A} , whose coverage guarantee also varies by models. (2) The rate of convergence of order $\mathcal{O}(\sqrt{\log(16T)/T} + \delta_T^{2/3})$ is a worst-case analysis for both marginal and conditional coverage. Empirical results show that even at a small training data size T , we have both marginal and conditional validity, which likely happens because \hat{f}_t are LOO ensemble predictors and thus approximate f well.

3.2 Convergence to oracle prediction interval

Our next goal is to establish the convergence rate of our estimated prediction interval \hat{C}_{T+1}^α to the oracle one C_{T+1}^α in (4). Define $\Delta : \mathbb{N} \rightarrow \mathbb{R}$ such that $\Delta(T) = \hat{C}_T^\alpha \Delta C_T^\alpha$: for any two subsets $A, B \subset \mathbb{R}$ under the Lebesgue measure μ , $A \Delta B := \mu(\{x \in \mathbb{R} : x \in A, x \notin B\}) + \mu(\{x \in \mathbb{R} : x \in B, x \notin A\})$. Theorem 3 shows that $\Delta(T)$ converges to 0 under Assumptions 1, 2 and regularity conditions, where the convergence rates are slower but at a similar order as that in Theorem 1.

Theorem 3 (Convergence to oracle prediction interval; errors are i.i.d.). *Suppose Assumption 1 and 2 hold. Furthermore, assume there exists a sequence $\{\gamma_T\}_{T \geq 1}$ that converges to zero such that $|f(x_{T+1}) - \hat{f}_{-(T+1)}(x_{T+1})| \leq \gamma_T$. Lastly, assume F_{T+1}^{-1} , \hat{F}_{T+1}^{-1} , and \hat{F}_{T+1} are Lipschitz continuous with constants K_{T+1} , K'_{T+1} , and K''_{T+1} respectively. We then have*

$$\Delta(T) \leq \gamma_T + \alpha K'_{T+1}/m + 2(K_{T+1} + M_{T+1})(12\sqrt{\log(16T)/T} + 2C\delta_T^{2/3}),$$

where m is the number of grids for line-search of $\hat{\beta}$ based on the past T prediction residuals and M_{T+1} is a constant that depends only on K_{T+1} and K''_{T+1} .

Finally, we would like to present a few remarks for all previous results:

Remark 2 (Width convergence under different error assumptions). *We note that when $\{\epsilon_t\}_{t=1}^T$ are not independent, Corollaries of Theorem 3 can be established, which will be similar to Corollaries 1 and 2. The underlying proof technique remains the same. More precisely, the rate $\sqrt{\log(16T)/T}$ will be replaced by $\log T/\sqrt{T}$ when errors follow linear processes and by $(\log T)^{2/3}/T^{1/3}$ when errors are strongly mixing with summable mixing coefficients.*

Remark 3 (Theorem wider applicability and caveats). *We comment on the wider applicability of Theorem 1, 2, 3, and the Corollaries. In general, the result also applies to other conformal prediction methods (for example, split conformal (Papadopoulos et al., 2007)), as long as the same assumptions hold. However, there is a major disadvantage when using split conformal and its variants that require a subset of training data as the “calibration data”. The value T on the right-hand side of Theorem 1, which is the size of full training data, becomes the size of the calibration data because prediction residuals are only computed on calibration data. The guarantees may thus become worse. Performance differences by these methods become more obvious in practice, especially when training data are relatively small*

comparing to the test data. In such cases, subsetting a part of the training data as calibration data is more impractical. Real-data examples that illustrate such cases are in Section 5.2.

Remark 4 (Coverage and interval convergence after $T + 1$). *In reality, it is likely that the error process $\{\epsilon_t\}_{t \geq 1}$ is non-stationary; the distribution functions may change at unknown times and the error dependencies can be different. Fortunately, results above are robust in such situations: suppose one uses the N past residuals to construct the prediction interval at time t . Firstly, the upper bound in Theorem 1 and 2 still hold, as long as (a) $\{\epsilon_i\}_{i=t-N}^{t-1}$ are independent (can be relaxed in the Corollaries) and distributed according to the common CDF F_t and (b) we can estimate the previous values $\{f(x_i)\}_{i=t-N}^{t-1}$ reasonably well as in Assumption 2. If in addition, we can approximate $f(x_t)$ well and the two inverse CDF functions are Lipschitz continuous, Theorem 3 holds. Therefore, our guarantees not only hold under non-stationary time-series $\{Y_t\}_{t \geq 1}$, but also hold under non-stationary errors $\{\epsilon_t\}_{t \geq 1}$.*

4. EnbPI Algorithm

We now present **EnbPI** in Algorithm 1, where \hat{f}^b is the b -th bootstrap estimator. We use superscript ϕ on variables to denote their dependence on ϕ . In Algorithm 1, Line 2, we use block bootstrap with T non-overlapping blocks, which is a popular method for bootstrapping dependent data (Kreiss and Paparoditis, 2011). The basic idea is to split the T training samples into l (non-)overlapping blocks, each with a size $\lfloor T/l \rfloor$. Then, sample from l blocks randomly with replacement.

We comment on the choice of hyperparameters as follows. (1) In general, \mathcal{A} can be a family of (parametric and non-parametric) prediction algorithms. (2) Different choice of aggregation functions ϕ brings different benefits, such as reducing the MSE under mean, avoiding sensitivity to outliers under median, or achieving both under trimmed mean. (3) As the number of pre-trained bootstrap models B increases, interval widths may be narrower. Empirically, we find choosing B between 20 and 50 is sufficient, especially for computationally intensive methods such as neural networks. (4) Larger s requires prediction further in the future without feedback; however, as s increases, the prediction becomes harder, which is reflected in that intervals become wider and the coverage deteriorates; how large s can be is determined by the dynamic of the data.

4.1 Properties of EnbPI

Computational efficiency. Note that in **EnbPI**, the prediction models in the ensemble are pre-trained once and stored; when deploying **EnbPI** for prediction, residuals are computed from T pre-trained models on the fly and the interval is constructed based on quantile values of T residuals. Thus, the main computation of **EnbPI** for obtaining the prediction interval is very small in calling the prediction algorithm \mathcal{A} B times. In comparison, the Jackknife+ approach (Barber et al., 2019b) requires requires B times training of \mathcal{A} on *each* leave- i -out sample $\{(x_j, y_j)\}_{j=1, j \neq i}^T$. This requires BT training of \mathcal{A} , which can be computationally intensive for complex prediction algorithms such as deep neural networks.

No overfitting or data splitting. Traditional CP methods such as split conformal (Papadopoulos et al., 2007) use data-splitting to avoid overfitting. In contrast, inspired by the J+aB

Algorithm 1 Ensemble batch prediction intervals (**EnbPI**)

Require: Training data $\{(x_i, y_i)\}_{i=1}^T$, prediction algorithm \mathcal{A} , significance level α , aggregation function ϕ , number of bootstrap models B , batch size s , and test data $\{(x_t, y_t)\}_{t=T+1}^{T+T_1}$; y_t is revealed as feedback only after prediction at t is done.

Ensure: Ensemble prediction intervals $\{C_t^{\phi, \alpha}(x_t)\}_{t=T+1}^{T+T_1}$

```

1: for  $b = 1, \dots, B$  do
2:   Sample with replacement an index set  $S_b = (i_1, \dots, i_T)$  from indices  $(1, \dots, T)$ .
3:   Compute  $\hat{f}^b = \mathcal{A}(\{(x_i, y_i) | i \in S_b\})$ .
4: end for
5: Initialize  $\hat{\epsilon} = \{\}$ 
6: for  $i = 1, \dots, T$  do
7:    $\hat{f}_{-i}^\phi(x_i) = \phi(\{\hat{f}^b(x_i) | i \notin S_b\})$ 
8:   Compute  $\hat{\epsilon}_i^\phi = y_i - \hat{f}_{-i}^\phi(x_i)$ 
9:    $\hat{\epsilon} = \hat{\epsilon} \cup \{\hat{\epsilon}_i^\phi\}$ 
10: end for
11: for  $t = T + 1, \dots, T + T_1$  do
12:    $\hat{f}_{-t}^\phi(x_t) = \phi(\{\hat{f}_{-i}^\phi(x_t)\}_{i=1}^T)$ 
13:   Compute  $\hat{\beta} = \arg \min_{\beta \in [0, \alpha]} ((1 - \alpha + \beta) \text{ quantile of } \hat{\epsilon} - \beta \text{ quantile of } \hat{\epsilon})$ 
14:    $w_{t, \text{lower}}^{\phi, \alpha} = \hat{\beta} \text{ quantile of } \hat{\epsilon}$ .
15:    $w_{t, \text{upper}}^{\phi, \alpha} = (1 - \alpha + \hat{\beta}) \text{ quantile of } \hat{\epsilon}$ .
16:   Return  $C_t^{\phi, \alpha}(x_t) = [\hat{f}_{-t}^\phi(x_t) + w_{t, \text{lower}}^{\phi, \alpha}, \hat{f}_{-t}^\phi(x_t) + w_{t, \text{upper}}^{\phi, \alpha}]$ 
17:   if  $t - T = 0 \bmod s$  then
18:     for  $j = t - s, \dots, t - 1$  do
19:       Compute  $\hat{\epsilon}_j^\phi = y_j - \hat{f}_{-j}^\phi(x_t)$ 
20:        $\hat{\epsilon} = (\hat{\epsilon} - \{\hat{\epsilon}_1^\phi\}) \cup \{\hat{\epsilon}_j^\phi\}$  and reset index of  $\hat{\epsilon}$ . {Sliding}
21:     end for
22:   end if
23: end for

```

procedure in (Kim et al., 2020), **EnbPI** trains LOO ensemble models on full data and avoids overfitting through thoughtful aggregations in lines 6-10. In particular, to construct the i -th LOO ensemble predictor, **EnbPI** aggregates all B bootstrap models that are *not* trained on the training datum (x_i, y_i) . Thus, the actual number of aggregated models is a Binomial random variable with parameters B and $(1 - 1/T)^T$; the Chernoff bound ensures that each ensemble predictor aggregates a balanced number of pre-trained models.

Leverage new data without model retraining. **EnbPI** constructs sequential prediction intervals without retraining \mathcal{A} . Instead, it leverages feedback by updating past residuals through a sliding window of size T , which adapts the interval widths to data and can handle change points (see Remark 1).

4.2 EnbPI on challenging tasks

We comment that **EnbPI** is flexible and can handle various challenging tasks.

Handle missing data. When training and/or test data have missing entries, we can properly increase the size of bootstrap samples to draw from the available training data — this is appropriate since we assume a common data model f . When deploying on test data, in case of **EnbPI** encountering a missing index t' , we impute the feature $x_{t'}$ if it is missing to compute the interval center and use the most recent T residuals to compute the interval width. For future prediction, the sliding window can skip over the residual $\epsilon_{t'}^\phi$ because $y_{t'}$ is unobserved. We may need to impute $y_{t'}$ for the *future* prediction at $t > t'$ if the feature x_t depends on $y_{t'}$. Section 5.3 illustrates the robust performance of **EnbPI** for missing data.

Network prediction. Consider a network with K nodes, so that the observations at node $k \in [K]$ are given by $\{(y_t^k, x_t^k)\}_{t \geq 1}$. To incorporate network temporal information, we define a new feature \tilde{x}_t^k at node k and time t as a collection of features from neighbors of k at time t and earlier. By adopting this setup, we can perform nodal prediction (from history and neighboring information) by applying our conformal prediction scheme; theoretical guarantees equally hold at each node as long as we use **EnbPI** for each node. We present an example of network prediction using the California solar radiation data in Appendix B.3.

Unsupervised anomaly detection. Suppose there is an anomalous point y_{t^*} at time t^* , due to either a change in model f at t^* or an unusually large stochastic error ϵ_{t^*} . As a result, y_{t^*} tends to lie far outside the interval (equivalently, $\epsilon_{t^*}^\phi$ is well below or above the $\hat{\beta}$ or $(1 - \alpha + \hat{\beta})$ quantile of past T residuals) and thus can be detected using the prediction interval. We present an example applying **EnbPI** to detect anomalous traffic flows in Section 5.4.

5. Experimental results

The experiments are organized as follows. In Section 5.1, we provide extensive simulations to examine the coverage and width of **EnbPI** intervals. In Section 5.2, we show that **EnbPI** attains valid marginal coverage on real data, whereas competing methods may fail. In Section 5.3, we present real-data experiments to examining the conditional coverage of **EnbPI**. In Section 5.4, we present an example for anomaly detection in traffic flow using **EnbPI**. In Appendix B.3 and B.4, we present more time-series data example to demonstrate that **EnbPI** has valid coverage and shorter intervals than the competing methods.

5.1 Simulation results

Setup. We examine the performance of **EnbPI** on different simulated experiments. In particular, for the model $Y_t = f(X_t) + \epsilon_t$ in (1), we consider three cases with increasing levels of model sophistication. We simulate 2000 data and use the first 1000 points to train the LOO ensemble predictors and the remaining 1000 points for testing (that is, $T = T_1 = 1000$):

- (1) Let $f(X_t) = \beta^T X_t$ be a linear model, where the entries of β and X_t are *i.i.d.* uniform distributed $U[0, 1]$; error ϵ_t are *i.i.d.* following the skewed normal distribution with mean μ , variance σ^2 , and skewness parameter a ; here let $a = 4, \mu = 0, \sigma^2 = 0.1$.
- (2) Let $f(X_t) = \beta^T X_t$, where 80% of β entries are zeros and observed entries are sampled *i.i.d.* from $U[0, 1]$. We choose $d = 1.6T$ so f is a high-dimensional sparse linear model; this model choice is inspired by Example 3.1 when discussing Assumption 2.

Meanwhile, let $X_t = Y_t^{-w}$ be the past w observations, so $Y_t^{-w} = [Y_{t-1}, \dots, Y_{t-w}]$; here $w = 100$ and we standardize X_t to have unit ℓ_2 norm. The errors are drawn from the same skewed normal distribution as above in (1).

- (3) Let $f(X_t) = (|\beta^T X_t| + (\beta^T X_t)^2 + |\beta^T X_t|^3)^{1/2}$, where β vector is generated the same as (2). Meanwhile, let $X_t = Y_t^{-w}$ and sample the errors ϵ_t from an AR(1) process, so that $\epsilon_t = \rho\epsilon_{t-1} + e_t$ and e_t are *i.i.d.* normal random variables with zero mean and unit variance with $\rho = 0.6$. It is known that the AR(1) process is strongly mixing, as long as e_t are *i.i.d.* with a nontrivial absolutely continuous component and $\mathbb{E}[(\log |e_t|)^+]$ is finite (Athreya and Pantula, 1986).

Hyperparameters to **EnbPI** are as follows: $\alpha = 0.05$, the aggregation ϕ takes the mean of the ensemble predictors, $B = 50, s = 1$. Thus, we build intervals aiming to cover 95% of test observations using 50 bagging estimators and slide the prediction interval every time we make a prediction. We consider prediction algorithms \mathcal{A} as linear regression without intercept from **sklearn**, lasso with $\alpha = 1$ from **sklearn**, and a neural network, respectively. The neural network is described in Appendix B.1. When doing the experiments, we did not optimize the performance of different prediction algorithms to demonstrate that **EnbPI** works well even under default settings.

Results. Figure 1 examines the marginal and conditional validity, as well as the interval width. The marginal coverage is obtained by averaging over T_1 test data and the conditional coverage is obtained by averaging over K randomly sampled errors $\{\epsilon_{T+1,i}\}_{i=1}^K$ by fixing $f(x_{T+1})$. Here $K = 100$. The left column in Figures 1(a)-(f) show the marginal coverage and width over different training sample sizes for the three cases. The dashed line with a bold blue label is the oracle interval width. We see that the marginal coverage in red is almost always valid at $1 - \alpha$ regardless of the sample size T , indicating **EnbPI** is suitable for small-sample problems. Meanwhile, interval width converges to the oracle width as the training sample size grows, validating Theorem 3. To examine the behavior of prediction intervals over time, the right column in Figures 1(a)-(f) show that prediction intervals follow data dynamics and cover the unknown Y_t with high probability. Moreover, Figures 1(g)-(i) illustrate that **EnbPI** always attains the conditional validity regardless of the sample size; set α to be 0.1. Despite a significant over-coverage, **EnbPI** intervals still approach the oracle, quantifying uncertainty more precisely as the training sample size grows.

Simulation with a noisy helix trajectory. Consider Y_t given by a nonlinear mapping of components of a helix in three-dimensional space contaminated by noise: $X_t = [r \cos(\theta_t), r \sin(\theta_t), H\theta_t]$, $f(X_t) = r \cos(\theta_t) \cdot (|r \sin(\theta_t)|)^{1/2} \cdot (H\theta_t + \varepsilon)^{-1/2}$, $\varepsilon = 10^{-3}$, and $\epsilon_t = \rho\epsilon_{t-1} + e_t$ where $\rho = 0.6$ and e_t are *i.i.d.* normal random variables with zero mean and unit variance. The color map of the helix is proportional to Y_t . We fix $H = 3, r = 10$ and generate 1000 samples parametrized by θ_t , which are uniformly spaced between 0 and 8π . The first 500 data points are used for training **EnbPI** with random forest regression (RF) and the rest 500 are used for testing. The RF setup is described in Appendix B.1. In Figure 2, we see that in the test phase intervals by **EnbPI** tightly cover the unknown response Y_t . Moreover, the blue and orange curves corresponding to \hat{Y}_t and Y_t are very close, which indicates that LOO ensemble predictors approximate the unknown model f very well.

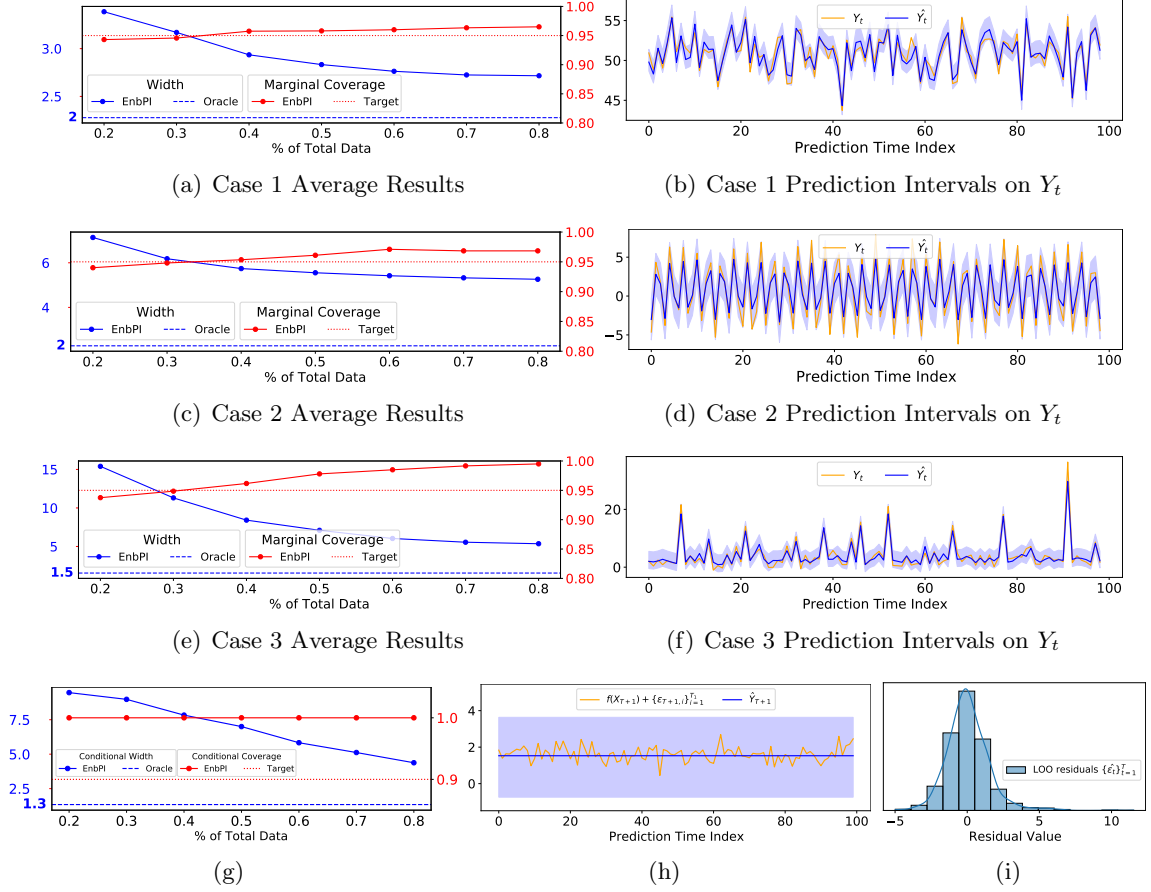


Figure 1: Simulation results. Figures (a)-(f) show marginal coverage, in which the blue dashed dotted line on the left is the oracle interval width. Prediction intervals in shaded blue are on the right. Figures (g)-(i) show conditional coverage in case 3 on the first test point, by repeatedly sampling the errors at $T + 1$.

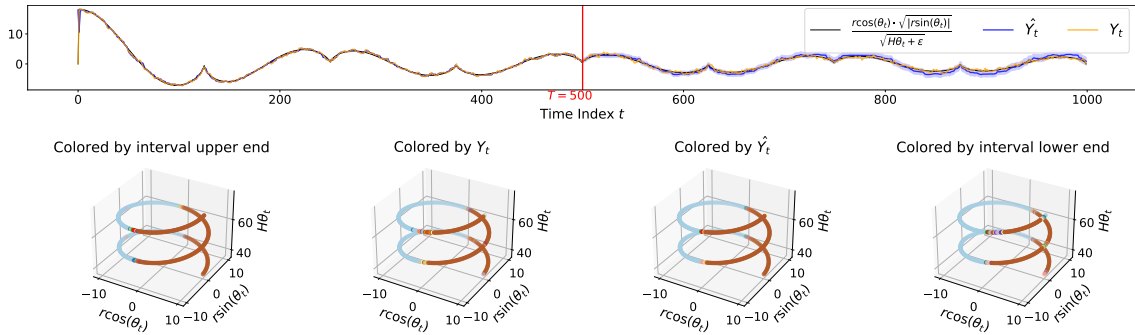


Figure 2: Helix colored by Y_t . Since values of Y_t are contained in prediction intervals with high probability and intervals are very narrow (top row), we see that the predicted colors closely match the actual color.

5.2 Real-data: Marginal validity and the interval width

In this section, we consider prediction for renewable energy generation. In this setting, the prediction and uncertainty quantification is critical due to their high stochasticity and non-stationarity.

Data description. The renewable energy data are from the National Solar Radiation Database and the Hackberry wind farm in Austin². We use 2018 hourly solar radiation data from Atlanta and nine cities in California and 2019 hourly wind energy data. In total, there are 11 time-series from 11 sensors (one from each sensor), and each time-series contains 8760 recordings (24×365), with other features such as temperature, humidity, wind speed, etc. In particular, California solar data constitute a network, where each node is a sensor. See Appendix B.1 for detailed data descriptions. From now on, we call X_t *univariate* if it is the history of Y_t and *multivariate* if it contains other features that predict Y_t .

Comparison methods. We primarily compare **EnbPI** with traditional time-series methods and two other CP methods. In Appendix B.2, we also compare **EnbPI** with the J+aB (Kim et al., 2020). The time-series methods are ARIMA(10,1,10), Exponential Smoothing (ExpSmoothing), and Dynamic Factor model (DynamicFactor). The CP methods are split/inductive conformal predictor (ICP) (Papadopoulos et al., 2007) and the weighted ICP (WeightedICP) (Tibshirani et al., 2019), where we split the data into 50% for training and 50% for calibration for both methods. Appendix B.1 describes their set up. We acknowledge that CP methods for time-series are currently lacking so that WeightedICP is chosen as a natural competitor among those that work beyond purely exchangeable data.

Prediction algorithm \mathcal{A} . We choose four prediction algorithms: ridge regression, random forest (RF), neural networks (NN), and recurrent neural networks (RNN) with LSTM layers. The first two are implemented in the Python **sklearn** library, and the last two are built using the **keras** library. See Appendix B.1 for their specifications.

Other hyperparameters. Since the three CP methods are trained on random subsets of training data, we repeat all experiments below for ten trials with independent random split in each trial. The time-series methods are only applied once on training data because they do not use random subsets. Throughout this subsection, we fix $s = 1$. Let $\alpha = 0.1$ and use the first 20% of the total hourly data for training unless otherwise specified. This creates small training samples for a challenging long-term predictive inference task. We use **EnbPI** under $B = 50$ and ϕ as taking the sample mean.

Results. All results in Section 5.2 and 5.3 come from using the Atlanta solar data. Similar results using California solar data and Hackberry wind data are in Appendix B.3. Figure 3 compares average coverage and width versus $1 - \alpha$ under **EnbPI** with different regression models and time-series methods. It is clear that **EnbPI** maintains coverage under any regression model we have chosen and both coverage and width have small standard errors. In contrast, coverage failure by ARIMA is more severe as $1 - \alpha$ increases. Although ARIMA intervals are much shorter in terms of widths than those by **EnbPI**, the severe coverage failure by ARIMA makes such benefits not meaningful. In addition, the other two time-series

2. NSRDB: <https://nsrdb.nrel.gov/>. Wind farm: <https://github.com/Duvey314/austin-green-energy-predictor>

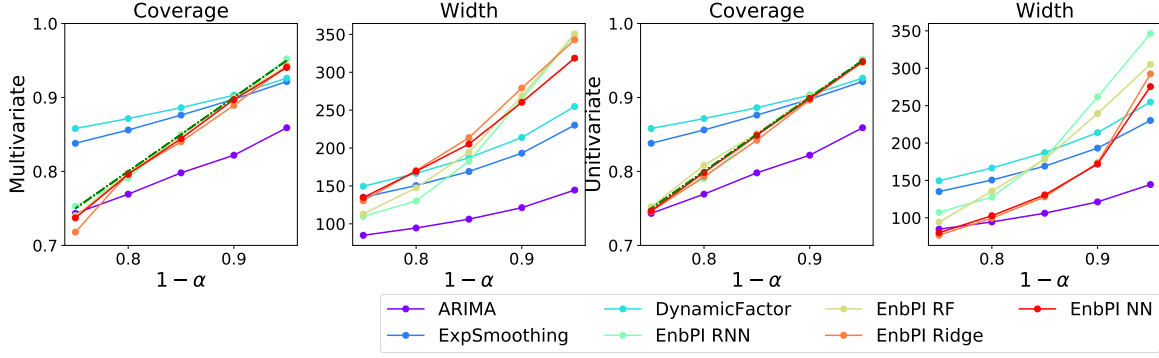


Figure 3: Solar power prediction in Atlanta. Average coverage and width versus $1 - \alpha$ target coverage by **EnbPI** under different prediction algorithms and by ARIMA, Exponential Smoothing, and Dynamic Factor Models. Five equally spaced $1 - \alpha \in [0.75, 0.95]$ are chosen, and **EnbPI** results are shaded with one standard error. The green dash-dotted line at 0.9 represents the target coverage.

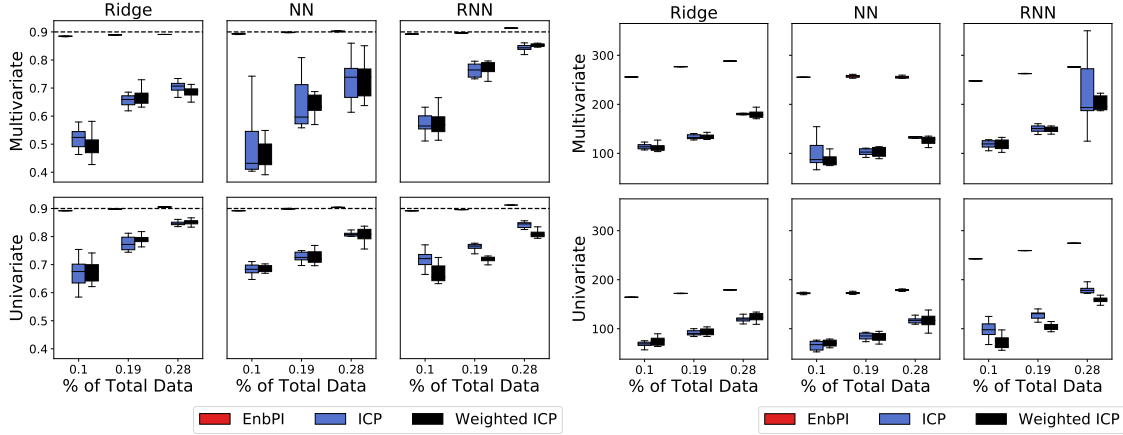


Figure 4: Solar power prediction in Atlanta. Boxplots of average coverage (top) and width (bottom) by **EnbPI**, **ICP**, and **WeightedICP**, whose training data vary as a percentage of total data (x -axis). Each box contains results from 10 independent trials. The black dash dotted line at 0.9 indicates target coverage.

methods cover above $1 - \alpha$ when α is large, but intervals are on average wider than those by **EnbPI** under ridge and NN if X_t is univariate; they both undercover when $1 - \alpha$ is large (for example, 95% target coverage). In summary, ensuring $1 - \alpha$ coverage under small α values is important in reality, making these methods not easily applicable for such time series.

Figure 4 compares grouped boxplots of coverage and width for CP methods using ridge, NN, and RNN. All coverage boxes by **EnbPI** tightly center around the target coverage and have a small variance. Moreover, **EnbPI** is very suitable for small-sample problems since its coverage barely varies across different training data sizes. On the other hand, **ICP** and

WeightedICP show significant under coverage, regardless of whether X_t is multivariate or univariate. Thus, they are neither valid nor applicable to time-series data. In terms of width, although intervals by ICP and WeightedICP are much shorter than **EnbPI**, the severe coverage failure by the former two methods makes such benefits not meaningful. On the other hand, **EnbPI** intervals under univariate X_t are shorter than those under multivariate ones, likely because response series’ historical observations are more predictive of the current value than available feature information. In retrospect, ICP or WeightedICP fails to cover well because their prediction intervals are not dynamically updated; widths are computed only on calibration data rather than updated by leveraging feedback. In particular, Figure 9 in the appendix illustrates how no sliding clearly decreases coverage validity even for **EnbPI** under a slightly different setting.

5.3 Real-data: Missing data, conditional coverage

In this section, we move beyond marginal coverage with two particular goals. Firstly, we aim to show conditional validity of **EnbPI** as it looks ahead beyond one step to construct multiple prediction intervals before receiving feedback (that is, $s > 1$). Secondly, we show that **EnbPI** can handle time-series with missing data, which commonly exist in reality. We choose only to use **EnbPI** for these tasks because it is the most stable method based on earlier results.

Setup. All hyperparameters into **EnbPI** except choices of s are kept the same unless otherwise specified. We fit **EnbPI** separately on subsets of hourly data, given that radiation data exhibit significant periodic variations (for example, recordings near noon have much larger magnitudes than the rest). More precisely, we fit **EnbPI** with NN once on data between 10 AM — 2 PM and once on data from the rest 5 hours, as only hours between 9 AM and 6 PM have radiation recordings. Let $s = 5$ hours, so **EnbPI** constructs five-hour ahead prediction intervals at most, after which the conditional coverage is computed separately at each hour. To create a more challenging missing data situation, we randomly drop 25% of both training and test data. As X_t may contain the history of Y_t for prediction, we impute missing entries as independent random samples from a normal distribution, whose mean and variance parameters are empirical mean and standard error of the most recent s observations. We assume exogenous features (for example, temperature, humidity, wind speed, etc.) are readily available and perform no imputation on them. The training data come from the first 92 days of observation (January-March), and intervals always lie within $[0, \infty)$, as solar radiation value cannot be negative. For clarity, we will only show results under one trial, and they hardly vary across trials.

Results. Figure 5 shows conditional coverage of **EnbPI** under NN. We title each subfigure by the hour, in which the bottom row visualizes the coverage over a sliding window to illustrate how **EnbPI** performance evolves. Several things are noticeable. Firstly, empirical distributions of LOO residuals in the rightmost figures are asymmetric around 0, justifying the need to build asymmetric intervals in **EnbPI**. Secondly, **EnbPI** can nearly obtain conditional coverage at all these hours, even with missing data, demonstrating its robustness. We note that the sliding coverage can be much poorer near the summer (for example, in August), likely because radiation data near the summer experience unknown shifts in the model f and violate our assumption for the data-generating process. Lastly, applying **EnbPI** separately

onto group training data that are more “similar” (for example, by morning and afternoon) can be essential, especially when the data-generating processes are heterogeneous over subgroups. In general, we believe **EnbPI** can obtain conditionally valid coverage on real data even in missing data. In Appendix B.2, we show more results when no feedback is available to **EnbPI** (that is, $s = \infty$), illustrating the necessity to slide past residuals for a dynamic interval calibration.³

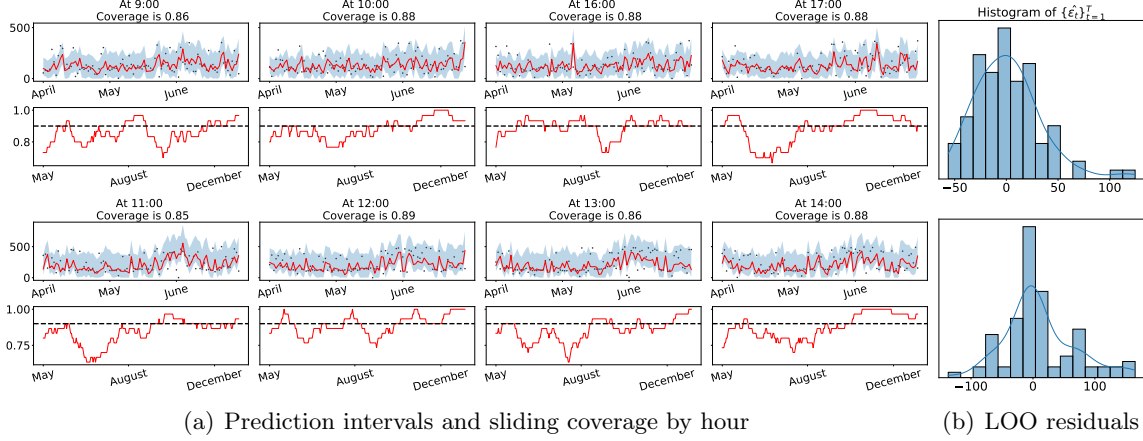


Figure 5: Solar power prediction in Atlanta, when **EnbPI** looks ahead beyond one step. The top figure at each hour in (a) visualizes observations in black, estimates in red, and prediction intervals in blue for three months (April-June). The bottom ones in (a) computes coverage using a sliding window of 30 days. The sliding coverage is much poorer near summertime (for example, August), when the data distribution may differ. Figure (b) visualizes histograms of asymmetrically distributed residuals used to compute interval widths at all hours on the same row.

5.4 Real data: Unsupervised anomaly detection

In this section, we use **EnbPI** to detect anomalies in traffic flow observations with missing data. In this setting, it is important to dynamically update decision thresholds (for example, upper and lower ends of prediction intervals) based on spatial and temporal information in the traffic sensor network because traffic data are highly correlated and non-stationary.

Data Description. The raw bi-hourly traffic flow data are from the California Department of Transportation⁴. Observations come from 10 sensors that are non-uniformly spaced in space. Each sensor has a pair of scaled latitude and longitude coordinates so that the ℓ_2 distance between any two sensors is within $[0, 1]$; the coordinates are used to define nodal neighbors. We randomly omit 30% of the training data at each sensor to create missing data. Unless otherwise specified, data from the first six months are for training, and the rest are for testing. See Appendix B.5 for detailed data description and how **EnbPI** is used.

3. For datasets with fixed sizes, $s = \infty$ is replaced by the length of the test data.

4. <https://pems.dot.ca.gov/>

Setup and comparison methods. Our goal is to identify binary anomalies at each sensor, defined as traffic flow observations with extremely large or small magnitude compared to those from its neighbor and/or in the past. It is natural to use our conformal prediction method as the whole data constitute a traffic network, and **EnbPI** can easily capture the spatio-temporal information. We compute the standard precision, recall, and F_1 score at each node; methods with higher F_1 scores are preferable for performance metrics. We compare **EnbPI** under four prediction algorithms used in Section 5.2 and 5.3 with eight competing anomaly detectors, four of which are unsupervised (for example, IForest, PCA, OCSVM, and HBOS), and the other four are supervised (for example, MLPClassifier, GBoosting, KNN, SVC). See Appendix B.5 for detailed description and parameter setup for the competitors. We build 15 pre-trained bootstrap models in **EnbPI**, fix the significance level α at 0.05, and use the mean aggregation function to build LOO ensemble predictors.

Results. Figure 6 compares all methods on a particular traffic sensor as we vary the size of training data. It is clear that **EnbPI** consistently obtains the highest F_1 scores when RNN is used as the prediction model; F_1 scores by **EnbPI** also are consistent across over training sample sizes. In addition, Table 1 shows the results with more sensors, from which **EnbPI** under NN or RNN still outperforms the other competitors by a large margin. In the future, we will consider multiple testing corrections to improve the performance (Bates et al., 2021; Chen and Kasiviswanathan, 2020; Ramdas et al., 2017), where the critical step is to examine the dependency of p -value as a correction step.

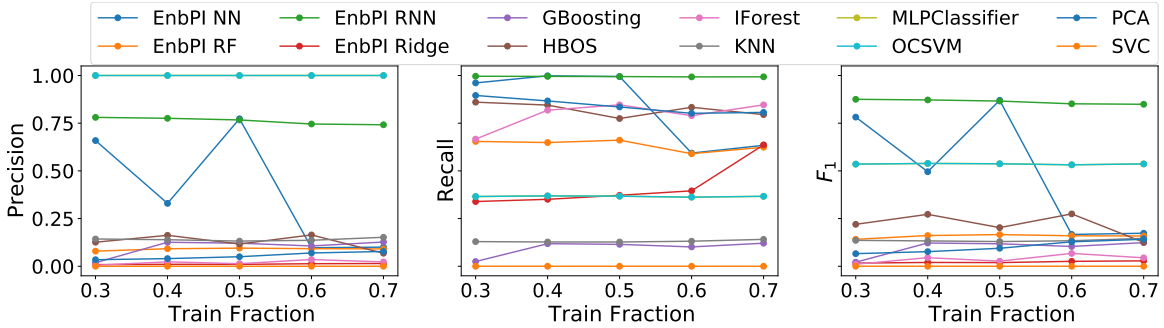


Figure 6: Traffic flow anomaly detection. Precision, Recall, and F_1 scores versus different amounts of training data (as percentages of total data) for different detectors. **EnbPI** under RNN and NN outperforms the other methods.

6. Conformal prediction under change points

In real applications, there can exist abrupt changes in the underlying data distribution, which are called *change points* (Xie et al., 2021; Aminikhanghahi and Cook, 2017). In this section, we present numerical experiments to demonstrate the performance of **EnbPI** in the presence of change points. We also discuss the potential adaption of **EnbPI** for change point detection.

We consider a change point happening during the testing phase and follow the setup in Section 5.1. Assume a change point at $T^* = 0.6(T + T_1)$, which alters the underlying model

Sensor (Anomaly Fraction)					282 (36%)	248 (27%)	151 (41%)	235 (29%)					
		F ₁ Score											
Detector		EnbPI Ridge	EnbPI RF	EnbPI NN	EnbPI RNN	HBOS	IForest	OCSVM	PCA	SVC	GBoosting	KNN	MLPClassifier
Sensor	282	0.13	0.14	0.88	0.88	0.16	0.02	0.51	0.09	0.0	0.04	0.07	0.51
	248	0.02	0.17	0.87	0.87	0.20	0.03	0.54	0.09	0.0	0.12	0.13	0.54
	151	0.02	0.14	0.81	0.80	0.11	0.04	0.39	0.08	0.0	0.08	0.12	0.39
	235	0.57	0.59	0.77	0.77	0.01	0.00	0.45	0.00	0.0	0.23	0.24	0.45
		Precision											
Detector		EnbPI Ridge	EnbPI RF	EnbPI NN	EnbPI RNN	HBOS	IForest	OCSVM	PCA	SVC	GBoosting	KNN	MLPClassifier
Sensor	282	0.46	0.59	0.96	0.96	0.58	0.71	0.34	0.75	0.0	0.04	0.07	0.34
	248	0.37	0.66	0.99	0.99	0.77	0.85	0.37	0.84	0.0	0.11	0.13	0.37
	151	0.24	0.61	0.96	0.96	0.30	0.47	0.24	0.46	0.0	0.08	0.11	0.24
	235	0.60	0.60	0.70	0.70	0.04	0.03	0.29	0.00	0.0	0.23	0.24	0.29
		Recall											
Detector		EnbPI Ridge	EnbPI RF	EnbPI NN	EnbPI RNN	HBOS	IForest	OCSVM	PCA	SVC	GBoosting	KNN	MLPClassifier
Sensor	282	0.07	0.08	0.81	0.81	0.10	0.01	1.0	0.05	0.0	0.04	0.07	1.0
	248	0.01	0.09	0.77	0.77	0.12	0.01	1.0	0.05	0.0	0.12	0.13	1.0
	151	0.01	0.08	0.69	0.68	0.07	0.02	1.0	0.04	0.0	0.09	0.12	1.0
	235	0.55	0.59	0.87	0.87	0.01	0.00	1.0	0.00	0.0	0.24	0.24	1.0

Table 1: Traffic flow anomaly detection. F_1 scores, Precision, and Recall by 12 methods on several selected sensors. Bold cells indicate the highest scores. **EnbPI** RNN or NN are better on this task in terms of F_1 scores.

f for the last 40% test data. As a result, the post-change responses Y_t are very different from the pre-change ones. We call the post-change model f_1 . For the linear model, let $f_1(X_t) = \beta_1 X_t$ and β_1 be entry-wise *i.i.d.* $U[0, 5]$. Recall the pre-change β is entry-wise *i.i.d.* $U[0, 1]$. For the high-dimensional sparse linear model, β_1 has twice many non-zero components as that of β and the components are drawn from $U[0, 1]$ independently. For the nonlinear model, we keep the same β but square the value $f(X_t)$. Choices of X_t and ϵ_t remain the same in each case.

Recall T is the length of the pre-change training data; let $T = 0.3(T + T_1) = 600$. To adapt to post-change dynamics as quickly as possible, we retrain the prediction algorithm on $0.1T$ data after the change point T^* . We assume the T^* is known to us (for instance, we can be detected and estimated using a change point detection algorithm (Xie et al., 2021)).

Figure 7 plots prediction intervals on top of actual data for three cases. Firstly, except for data indexed between T^* and $T^* + 0.1T$, most prediction data from both pre-change and post-change models are covered by **EnbPI** intervals. Secondly, prediction intervals built with pre-change models on post-change data tend to have much wider widths than other ones, reflecting a poor estimation of \hat{f} by the pre-change models. Lastly, the lower ends of prediction intervals after $T^* + 0.1T$ are very loose for Case 3. This is likely because LOO ensemble neural networks are trained only on 60 post-change data, which can be remedied by collecting more post-change data before refitting estimators.

One can potentially adapt **EnbPI** to detect change points. From Figure 7, we observe that the change point leads to unusually wide post-change prediction intervals. As a result, one should monitor *both* the evolution of interval widths *and* coverage performances. On the one hand, when only f changes but the distribution of errors remains the same, the interval tends to be wider, but the coverage is poorer. On the other hand, if f remains the

same but the distribution changes, intervals may also become wider. However, coverage may not be as greatly affected because estimators by **EnbPI** can approximate f well. Due to a sliding window over residuals, one can adapt to the post-change distribution. These ideas resonate with several other works: Gibbs and Candès (2021) construct prediction sets under distribution shifts sequentially and prove that when shifts are small, the marginal coverage is approximately maintained. As a result, when coverage is significantly less than $1 - \alpha$, it can indicate an abrupt shift in distribution. Such ideas may also be used to test whether the test distribution lies in an f -divergence ball of the training distribution, given i.i.d. training and test data from the corresponding distribution (Cauchois et al., 2020); extensions to time series remain unexplored. On the other hand, a line of works (Vovk, 2020, 2021; Vovk et al., 2021) builds martingales to detect change points which however, violates data exchangeability. The lower bound for the average-run-length is established for the Shiryaev–Roberts procedure using such martingale (Vovk, 2020, Proposition 4.1). How to extend the ideas beyond testing exchangeable data remains an open question.

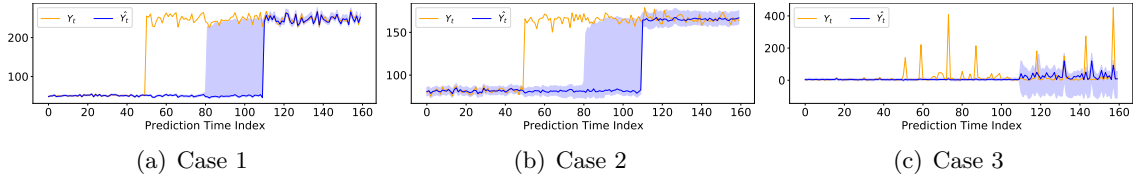


Figure 7: Simulation with a change point at $T^* = 1200$. We overlay prediction intervals in shaded blue on top of the actual data and plot 50 predictions before T^* and after refitting \mathcal{A} with 60 post-change data. Collecting more post-change data to fit **EnbPI** will yet better estimation with tighter prediction intervals.

7. Conclusions and Discussions

In this paper, we present a predictive inference method for dynamic time series. Theoretically, we can show that the constructed intervals are asymptotically valid without assuming data exchangeability: relaxing this requirement is crucial for time series data, and the interval width converges to the oracle one. We also present a simple, computationally friendly, and interpretable algorithm called **EnbPI**, which is an efficient ensemble-based wrapper for many prediction algorithms, including deep neural networks. Empirically, it works well on time series from various applications, including network data and data with missing entries, and maintains validity when other predictive inference methods fail. Furthermore, one can use **EnbPI** for unsupervised sequential anomaly detection. While the theoretical guarantee of **EnbPI** requires consistent estimation of the true model, empirical results are valid even under potentially misspecified models, and coverage is almost always valid.

Future work includes several possible directions. We may adapt **EnbPI** for classification problems (Angelopoulos et al., 2020; Romano et al., 2020) by defining conformity scores other than residuals. It can also be interesting to further develop **EnbPI** for online change point detection and adaptation for time series, extending the idea of sequential testing of data exchangeability (Volkhovskiy et al., 2017) based on the Shiryaev-Roberts procedure.

Acknowledgments

The work is partially supported by NSF CAREER CCF-1650913, CMMI-2015787, DMS-2134037, DMS-1938106, and DMS-1830210.

Appendix A. Proofs

For notation simplicity, we remove subscripts $T + 1$ for \hat{F} , \tilde{F} , and F .

Proof of Lemma 1. When the error process is i.i.d., the famous Dvoretzky–Kiefer–Wolfowitz inequality (Kosorok, 2007, p.210) implies that

$$\mathbb{P}(\sup_x |\tilde{F}(x) - F(x)| > x_T) \leq 2e^{-2Tx_T^2}.$$

Pick $s_T = \frac{\sqrt{W(16T)}}{2\sqrt{T}}$, where $W(T)$ is the Lambert W function that satisfies $W(T)e^{W(T)} = T$. We see that $s_T \leq \sqrt{\log(16T)/T}$. Thus, define the event A_T on which $\sup_x |\tilde{F}(x) - F(x)| \leq \sqrt{\log(16T)/T}$, whereby we have

$$\begin{aligned} \sup_x |\tilde{F}(x) - F(x)| \Big| A_T &\leq \sqrt{\log(16T)/T} \\ P(A_T^C) &\leq \sqrt{\log(16T)/T}. \end{aligned}$$

Furthermore, note that

$$\begin{aligned} &\sup_x |\tilde{F}(x) - F(x)| \\ &\stackrel{(i)}{=} \mathbb{P}(F(\epsilon_{T+1}) \leq \sup_x |\tilde{F}(x) - F(x)|) \\ &= P([F(\epsilon_{T+1}) \leq \sup_x |\tilde{F}(x) - F(x)|] \cap A_T) + P([F(\epsilon_{T+1}) \leq \sup_x |\tilde{F}(x) - F(x)|] \cap A_T^C) \\ &\leq P(F(\epsilon_{T+1}) \leq \sup_x |\tilde{F}(x) - F(x)| \Big| A_T) + P(A_T^C) \\ &\stackrel{(ii)}{=} \sup_x |\tilde{F}(x) - F(x)| \Big| A_T + P(A_T^C), \end{aligned}$$

where (i) holds because $F(\epsilon_{T+1}) \sim \text{Unif}[0, 1]$ and $\sup_x |\tilde{F}(x) - F(x)| \in [0, 1]$, and (ii) holds because $F(\epsilon_{T+1}) \sim \text{Unif}[0, 1]$ and the distribution of $F(\epsilon_{T+1})$ is unaffected by the bound on $\sup_x |\tilde{F}(x) - F(x)|$ conditioning on A_T . Thus, we can provide a deterministic bound on $\sup_x |\tilde{F}(x) - F(x)|$ for any T . \square

Proof of Lemma 2. Note that Assumption 2 is equivalent to requiring $\sum_{i=1}^T (\hat{\epsilon}_i - \epsilon_i)^2 \leq \delta_T^2$. Thus, let $S := \{i \in [T] : |\hat{\epsilon}_i - \epsilon_i| \geq \delta_T^{2/3}\}$. It follows that

$$|S|\delta_T^{4/3} \leq \sum_{i=1}^T (\hat{\epsilon}_i - \epsilon_i)^2 \leq T\delta_T^2,$$

where the second inequality follows by the first condition in Assumption 2. As a result, $|S| \leq T\delta_T^{2/3}$ and we see that for any $x \in \mathbb{R}$,

$$\begin{aligned}
|\hat{F}(x) - \tilde{F}(x)| &\leq \frac{1}{T} \sum_i |\mathbf{1}\{\hat{\epsilon}_i \leq x\} - \mathbf{1}\{\epsilon_i \leq x\}| \\
&\stackrel{(i)}{\leq} \frac{1}{T} (|S| + \sum_{i \notin S} |\mathbf{1}\{\hat{\epsilon}_i \leq x\} - \mathbf{1}\{\epsilon_i \leq x\}|) \\
&\stackrel{(ii)}{\leq} \frac{1}{T} (|S| + \sum_{i \notin S} \mathbf{1}\{|\epsilon_i - x| \leq \delta_T^{2/3}\}) \\
&\leq \delta_T^{2/3} + \mathbb{P}(|\epsilon_{T+1} - x| \leq \delta_T^{2/3}) + \\
&\quad \sup_x \left| \frac{1}{T} \sum_{i \notin S} \mathbf{1}\{|\epsilon_i - x| \leq \delta_T^{2/3}\} - \mathbb{P}(|\epsilon_{T+1} - x| \leq \delta_T^{2/3}) \right| \\
&\stackrel{(iii)}{=} \delta_T^{2/3} + [F(x + \delta_T^{2/3}) - F(x - \delta_T^{2/3})] + \\
&\quad \sup_x [|\tilde{F}(x + \delta_T^{2/3}) - \tilde{F}(x - \delta_T^{2/3})| - |F(x + \delta_T^{2/3}) - F(x - \delta_T^{2/3})|] \\
&\leq (L_{T+1} + 1)\delta_T^{2/3} + 2 \sup_x |\tilde{F}(x) - F(x)|. \tag{6}
\end{aligned}$$

We remark that (i) follows as we analyze $i \in S$ and $i \notin S$ separately, (ii) follows since $|\mathbf{1}\{a \leq x\} - \mathbf{1}\{b \leq x\}| \leq \mathbf{1}\{|b - x| \leq |a - b|\}$ for any constant a, b and univariate x and $|\hat{\epsilon}_i - \epsilon_i| \leq \delta_T^{2/3}$ for $i \notin S$, and (iii) follows since we assume $\{\epsilon_t\}_{t=1}^T$ have the common CDF F . \square

Proof of Theorem 1. Recall the following definitions:

- $\hat{p}_{T+1} := \frac{1}{T} \sum_i \mathbf{1}\{\hat{\epsilon}_i \leq \hat{\epsilon}_{T+1}\}$, which is the empirical p -value defined using residuals.
- $\tilde{F}(x) := \frac{1}{T} \sum_{i=1}^T \mathbf{1}\{\epsilon_i \leq x\}$ as the empirical CDF of F . Equivalently define $\hat{F}(x)$ using prediction residuals $\hat{\epsilon}_i$.

As a consequence, for any $\beta \in [0, \alpha]$, the following are equivalent:

$$\begin{aligned}
&|\mathbb{P}(Y_{T+1} \in \hat{C}_{T+1}^\alpha | X_{T+1} = x_{T+1}) - (1 - \alpha)| \\
&\stackrel{(i)}{=} |\mathbb{P}(\beta \leq \hat{p}_{T+1} \leq 1 - \alpha + \beta) - (1 - \alpha)| \\
&= |\mathbb{P}(\beta \leq \hat{F}(\hat{\epsilon}_{T+1}) \leq 1 - \alpha + \beta) - \mathbb{P}(\beta \leq F(\epsilon_{T+1}) \leq 1 - \alpha + \beta)|, \tag{7}
\end{aligned}$$

where (i) follows by the equivalence we pointed out at the beginning of Section 3.1.

We can rewrite the right hand side of (7) as follows:

$$\begin{aligned}
 & |\mathbb{P}(\beta \leq \hat{F}(\hat{\epsilon}_{T+1}) \leq 1 - \alpha + \beta) - \mathbb{P}(\beta \leq F(\epsilon_{T+1}) \leq 1 - \alpha + \beta)| \\
 & \leq \mathbb{E}|\mathbf{1}\{\beta \leq \hat{F}(\hat{\epsilon}_{T+1}) \leq 1 - \alpha + \beta\} - \mathbf{1}\{\beta \leq F(\epsilon_{T+1}) \leq 1 - \alpha + \beta\}| \\
 & \stackrel{(i)}{\leq} \mathbb{E}(|\mathbf{1}\{\beta \leq \hat{F}(\hat{\epsilon}_{T+1})\} - \mathbf{1}\{\beta \leq F(\epsilon_{T+1})\}| + |\mathbf{1}\{\hat{F}(\hat{\epsilon}_{T+1}) \leq 1 - \alpha + \beta\} - \mathbf{1}\{F(\epsilon_{T+1}) \leq 1 - \alpha + \beta\}|) \\
 & \stackrel{(ii)}{\leq} \mathbb{P}(|F(\epsilon_{T+1}) - \beta| \leq |\hat{F}(\hat{\epsilon}_{T+1}) - F(\epsilon_{T+1})|) + \mathbb{P}(|F(\epsilon_{T+1}) - (1 - \alpha + \beta)| \leq |\hat{F}(\hat{\epsilon}_{T+1}) - F(\epsilon_{T+1})|) \\
 & \stackrel{(iii)}{=} 4|\hat{F}(|\hat{\epsilon}_{T+1}|) - F(|\epsilon_{T+1}|)| \\
 & \leq 4|\hat{F}(|\hat{\epsilon}_{T+1}|) - \tilde{F}(|\epsilon_{T+1}|)| + 4|\tilde{F}(|\epsilon_{T+1}|) - F(|\epsilon_{T+1}|)| \\
 & \leq 4\sup_x |\hat{F}(x) - \tilde{F}(x)| + 4\sup_x |\tilde{F}(x) - F(x)|,
 \end{aligned}$$

where inequality (i) follows since for any constants a, b and univariates x, y , $|\mathbf{1}\{a \leq x \leq b\} - \mathbf{1}\{a \leq y \leq b\}| \leq |\mathbf{1}\{a \leq x\} - \mathbf{1}\{a \leq y\}| + |\mathbf{1}\{x \leq b\} - \mathbf{1}\{y \leq b\}|$. Moreover, inequality (ii) follows since $|\mathbf{1}\{a \leq x\} - \mathbf{1}\{b \leq x\}| \leq \mathbf{1}\{|b - x| \leq |a - b|\}$ for any constant a, b and univariate x and $\mathbb{E}[\mathbf{1}\{A\}] = \mathbb{P}(A)$. Lastly, inequality (iii) follows because the distribution of $F(\epsilon_{T+1})$ is $\text{Unif}[0, 1]$.

Since Lemma 1 says

$$\begin{aligned}
 \sup_x |\tilde{F}(x) - F(x)| & \leq \sup_x |\tilde{F}(x) - F(x)| \Big|_{A_T} + P(A_T^C), \\
 \sup_x |\tilde{F}(x) - F(x)| \Big|_{A_T} & \leq \sqrt{\log(16T)/T}, \\
 P(A_T^C) & \leq \sqrt{\log(16T)/T}
 \end{aligned}$$

and Lemma 2 says

$$\sup_x |\hat{F}(x) - \tilde{F}(x)| \leq C\delta_T^{2/3} + 2\sup_x |\tilde{F}(x) - F(x)|,$$

we have that

$$4\sup_x |\hat{F}(x) - \tilde{F}(x)| + 4\sup_x |\tilde{F}(x) - F(x)| \leq 24\sqrt{\log(16T)/T} + 4C\delta_T^{2/3}$$

□

Based on the proof of Theorem 1, note that the following bound always hold under Assumption 2.

$$|\mathbb{P}(\beta \leq \hat{p}_{T+1} \leq 1 - \alpha + \beta) - (1 - \alpha)| \leq 24x_T + 4C\delta_T^{2/3},$$

where we want to find the appropriate sequences s_T and $g(s_T)$ satisfying $s_T = g(s_T)$ so that

$$\mathbb{P}(\sup_x |\tilde{F}(x) - F(x)| > s_T) \leq g(s_T).$$

As a result, proofs of Collaries to Theorem 1 reduce to finding x_T .

Assumption 3 (Errors follow Linear Processes). Assume $\{\epsilon_t\}_{t=1}^{T+1}$ satisfy $\epsilon_t = \sum_{j=1}^{\infty} \delta_j z_{t-j}$ for each i , under which z_{i-j} are i.i.d. with finite first absolute moment and δ_j are bounded in absolute value by some function g such that $\sum_{i=1}^{\infty} ig(i)$ converges. Moreover, assume $\{\epsilon_t\}_{t=1}^{T+1}$ are distributed according to the common CDF F , which is Lipschitz continuous with constant $L_{T+1} > 0$.

Proof of Corollary 1. Following these assumptions, Hesse (1990) proves that $\sup_x |\tilde{F}(x) - F(x)| = \mathcal{O}(\log T / \sqrt{T})$ (see Hesse, 1990, Theorem 3). This guarantee yields the desired result by letting $s_T \in \mathcal{O}(\log T / \sqrt{T})$. \square

Proof of Corollary 2. Define $v_T(x) := \sqrt{T}(\tilde{F}(x) - F(x))$. Then, Proposition 7.1 in (Rio, 2017) shows that

$$\mathbb{E}(\sup_x |v_T(x)|^2) \leq (1 + 4 \sum_{k=0}^T \alpha_k) (3 + \frac{\log T}{2 \log 2})^2,$$

where α_k is the k^{th} mixing coefficient. Since we assumed that the coefficients are summable with $\sum_{k \geq 0} \alpha_k < M$ (for example, $\alpha_k = \mathcal{O}(n^{-s})$, $s > 1$), Markov Inequality shows that

$$\begin{aligned} \mathbb{P}(\sup_z |\tilde{F}(x) - F(x)| \geq x_T) &\leq \frac{\mathbb{E}(\sup_x |v_T(x)|^2 / T)}{x_T^2} \\ &\leq \frac{1 + 4M}{Tx_T^2} (3 + \frac{\log T}{2 \log 2})^2. \end{aligned}$$

Thus, we let $s_T := \left(\frac{1+4M}{T} (3 + \frac{\log T}{2 \log 2})^2 \right)^{1/3} \approx \left(\frac{M(\log T)^2}{2T} \right)^{1/3}$ and see that

$$\mathbb{P} \left(\sup_x |\tilde{F}(x) - F(x)| \leq \left(\frac{M(\log T)^2}{2T} \right)^{1/3} \right) \geq 1 - \left(\frac{M(\log T)^2}{2T} \right)^{1/3}.$$

Now, define $C_1 := (M/2)^{1/3}$ and the event A_T on which $\sup_x |\tilde{F}(x) - F(x)| \leq C_1 (\log T)^{2/3} / T^{1/3}$, whereby we have

$$\begin{aligned} \sup_x |\tilde{F}(x) - F(x)| \Big|_{A_T} &\leq C_1 (\log T)^{2/3} / T^{1/3} \\ P(A_T^C) &\leq C_1 (\log T)^{2/3} / T^{1/3}. \end{aligned}$$

\square

Proof of Theorem 3. Define $\hat{F}^{-1}(\alpha) := \alpha$ quantile of $\{\hat{\epsilon}_i\}_{i=1}^T$ as the inverse empirical CDF of \hat{F} . Call $\hat{\beta}_{\text{line}}$ the estimator of $\hat{\beta}$ after line-search with m grids. By the form of C_t^α and \hat{C}_t^α , we have

$$\begin{aligned} \Delta(T) \leq & |f(X_t) - \hat{f}_{-t}(X_t)| + 2 \overbrace{(|\hat{F}^{-1}(1 - \alpha + \hat{\beta}_{\text{line}}) - \hat{F}^{-1}(1 - \alpha + \hat{\beta})|)}^{(i)} + \\ & \overbrace{(|\hat{F}^{-1}(1 - \alpha + \hat{\beta}) - F^{-1}(1 - \alpha + \hat{\beta})|)}^{(ii)} + \overbrace{(|F^{-1}(1 - \alpha + \hat{\beta}) - F^{-1}(1 - \alpha + \beta^*)|)}^{(iii)}, \end{aligned}$$

where (i) can be bounded under accurate binning with the Lipschitz continuity assumption on the inverse empirical CDF \hat{F}^{-1} , (ii) is a consequence of Theorem 1, and (iii) applies the bound of (ii) twice.

Proof of (i). Partition $[0, \alpha]$ into $m + 1$ equally spaced values $0, \alpha/m, 2\alpha/m, \dots, \alpha$. It is clear that the estimator $\hat{\beta}_{\text{line}}$ upon we iterating through these $m + 1$ values satisfies

$$|\hat{\beta}_{\text{line}} - \hat{\beta}| \leq \alpha/2m.$$

Therefore, the Lipschitz continuity of \hat{F}^{-1} guarantees that

$$|\hat{F}^{-1}(1 - \alpha + \hat{\beta}_{\text{line}}) - \hat{F}^{-1}(1 - \alpha + \hat{\beta})| \leq \alpha K'_{T+1}/2m.$$

Proof of (ii). We provide the rate of convergence of $\sup_{\alpha \in [0,1]} |F^{-1}(\alpha) - \hat{F}^{-1}(\alpha)|$ to zero.

For any $y \in [0, 1]$, let $x := \hat{F}^{-1}(y)$. We now have

$$\begin{aligned} |F^{-1}(y) - \hat{F}^{-1}(y)| &= |F^{-1}(\hat{F}(x)) - x| \\ &= |F^{-1}(\hat{F}(x)) - F^{-1}(F(x))| \\ &\stackrel{(a)}{\leq} K_{T+1} |\hat{F}(x) - F(x)| \\ &\leq K_{T+1} \sup_{x' \in \mathbb{R}} |\hat{F}(x') - F(x')|, \end{aligned}$$

where (a) holds by the Lipschitz continuity of F^{-1} . Now, Theorem 1 implies that

$$\sup_{x' \in \mathbb{R}} |\hat{F}(x') - F(x')| \leq 6\sqrt{\log(16T)/T} + C\delta_T^{2/3},$$

whereby we thus have

$$\sup_{\alpha \in [0,1]} |F^{-1}(\alpha) - \hat{F}^{-1}(\alpha)| \leq K_{T+1}(6\sqrt{\log(16T)/T} + C\delta_T^{2/3}).$$

Proof of (iii). Intuitively, we know that $\hat{\beta}$ converges to β^* , as a consequence of \hat{F}^{-1} converging to F^{-1} . We can indeed bound $\hat{\beta} - \beta^*$ by upper and lower bounding $|\hat{\beta} - \beta^*|$ as follows:

$$\begin{aligned} \hat{\beta} - \beta^* &\leq |\hat{\beta} - \beta^*| \\ &= \hat{F}(\hat{F}^{-1}(|\hat{\beta} - \beta^*|)) - \hat{F}(\hat{F}^{-1}(0)) \\ &\leq K''_{T+1}(\hat{F}^{-1}(|\hat{\beta} - \beta^*|) - \hat{F}^{-1}(0)). \end{aligned}$$

The last inequality follows from assuming \hat{F} is Lipschitz continuous with constant K''_{T+1} . The quantity $(\hat{F}^{-1}(|\hat{\beta} - \beta^*|) - \hat{F}^{-1}(0))$ is non-negative since $\hat{F}^{-1}(0)$ is by definition the minimum of \hat{F}^{-1} on $[0, 1]$. Similarly,

$$\begin{aligned} F^{-1}(\hat{\beta} - \beta^*) - F^{-1}(0) &\leq K_{T+1}(\hat{\beta} - \beta^*) \\ &\leq K_{T+1}|\hat{\beta} - \beta^*|. \end{aligned}$$

Similarly, the quantity $F^{-1}(\hat{\beta} - \beta^*) - F^{-1}(0)$ is also non-negative, since $F^{-1}(0)$ is by definition the minimum of F^{-1} on $[0, 1]$. As a result,

$$|\hat{\beta} - \beta^*| \leq \left(|\hat{F}^{-1}(|\hat{\beta} - \beta^*|) - F^{-1}(|\hat{\beta} - \beta^*|)| + |F^{-1}(0) - \hat{F}^{-1}(0)| \right) / (1/K_{T+1}'' - K_{T+1}),$$

which implies that $M := \frac{2K_{T+1}^2}{1/K_{T+1}'' - K_{T+1}}$ by Lipschitz continuity of F^{-1} .

□

Appendix B. More experiments

We provide a quick overview of how this section is organized: In Appendix B.1, we describe the renewable energy time-series, the competing methods to **EnbPI**, and the regression models \mathcal{A} . In Appendix B.2, we briefly compare **EnbPI** against J+aB (Kim et al., 2020) and mainly present multi-step ahead inference results on the Atlanta solar radiation data when $s = 5$ and $s = \infty$. In Appendix B.3, we test **EnbPI** on the network California solar data and Austin wind data, similar to those on Atlanta solar data from the main text. We first show the interval validity of **EnbPI** and then apply **EnbPI** on the more challenging multi-step ahead inference task when missing data are present. In Appendix B.4, we apply **EnbPI** on other datasets, such as greenhouse gas emission data, air pollution data, and appliances energy data. We observe that **EnbPI** rarely loses marginal validity and can produce shorter intervals than competing methods. We do not study multi-step ahead inference on these datasets as we primarily aim to demonstrate the applicability of **EnbPI**. In Section B.5, we describe the anomaly detection setup and then provide details of eight other competing anomaly detection methods.

B.1 Data, competing methods, and regression models

Data Description. The solar dataset is available at <https://nsrdb.nrel.gov/>. The 9 cities we chose are Fremont, Milpitas, Mountain View, North San Jose, Palo Alto, Redwood City, San Mateo, Santa Clara, Sunnyvale. The wind dataset is publically available at <https://github.com/Duvey314/austin-green-energy-predictor>.

*Competing methods to **EnbPI**.* Recall we compete **EnbPI** against ARIMA(10,1,10), Exponential Smoothing, Dynamic Factor model, split conformal predictor, and weighted split conformal predictor:

- The first three time-series methods are implemented in Python’s `statsmodel` package. The ARIMA model is used under default setting and the other two other methods include damped trend components and seasonal cycles of 24, because most data are updated hourly with daily periodicity.
- The WeightedICP is proven to work when the test distribution shifts in proportion to the training distribution; it generalizes to more complex settings than ICP. We use logistic regression to estimate the weights for WeightedICP.

Regression models \mathcal{A} . Below are the parameter specifications for the four baseline models \mathcal{A} , unless otherwise specified:

- For ridge, the penalty parameter α is chosen with generalized cross-validation over ten uniformly spaced grid points between 0.0001 to 10 (the package default α is 1). Higher α means more robust regularization.
- For RF, we build ten trees under the mean-squared-error (MSE) criterion. We restrict the maximum search depth of each tree to 2 for faster training. We only allow each tree to split features rather than samples so that combining RFs trained on subsets of the training data is reasonable for **EnbPI**.
- For NN, we add three hidden layers, each having 100 hidden nodes, and apply 20% dropout after the second hidden layer to avoid overfitting. We use the Relu activation between hidden layers. The optimizer is Adam with a fixed learning rate of 5×10^{-4} under the MSE loss. Batch size equals 10% of training data, and maximum epoch equals 250. We also use early stopping if there is no improvement in training error after ten epochs.
- For RNN, we add two hidden LSTM layers, followed by a dense output layer. Each LSTM layer has 100 hidden neurons, so the output from the first hidden layer is fed into the second hidden layer. We use the Tanh activation function for these two hidden layers and the Relu activation function for the dense layer. The optimizer is Adam with a fixed learning rate of 5×10^{-4} under the MSE loss. Batch size equals 10% of training data, and maximum epoch equals 10. We use early stopping if there is no improvement in training error after ten epochs.

B.2 Additional results on solar—Atlanta

Comparison with J+aB. Figure 8 makes it clear that unlike the other two methods (that is, Split conformal used in (Chernozhukov et al., 2018, 2020) and J+aB in (Kim et al., 2020)), **EnbPI** always retains marginally valid coverage under any regression model \mathcal{A} we considered.

Multi-step ahead inference when $s = \infty$. We train on the same set of data as in Figure 5. Since change points are present in the data (that is, data near summer have very different radiation levels from the training data), we expect **EnbPI** to perform less well if not slide. Indeed, Figure 9 shows poor conditional coverage, even if we train on the same set of data and further assume *no missing data exist*.

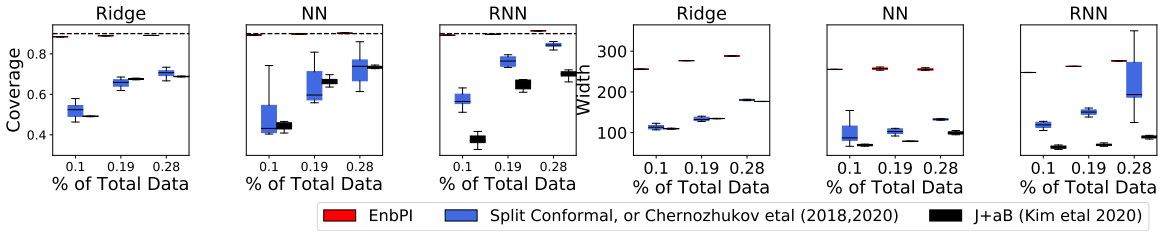


Figure 8: The setup is the same as Figure 4 in main text. Unlike the others, **EnbPI** almost always retains marginally valid coverage under any regression model \mathcal{A} we considered.

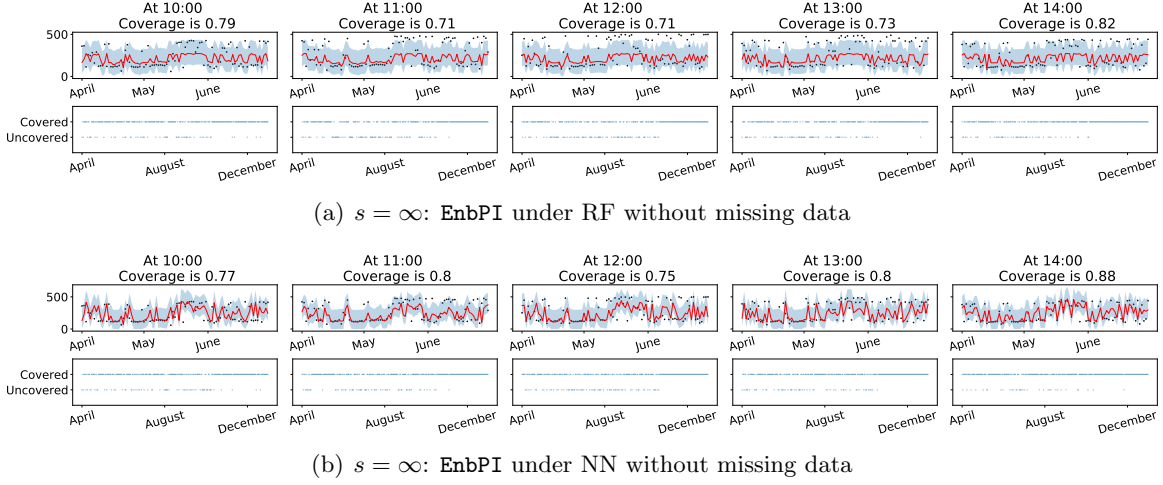


Figure 9: Solar power prediction in Atlanta when no feedback is available. The top figure at each hour visualizes observations in black, estimates in red, and prediction intervals in blue for three months (April–June). The bottom figure at each hour plots whether the prediction interval correctly covers the response during test (April–December). We observe clear decrease in conditional coverage even if no missing data is present and the same prediction models are used. This situation illustrates the necessity to updated past residuals based on new feedback.

B.3 Results on solar—California and wind—Austin

We note that in general, EnbPI on California solar data and on Austin wind data generates results very similar to those on Atlanta solar data. Therefore, we do not provide separate analyses of individual figures but highlight the overall pattern and differences in each part below.

A. Marginal validity and the interval width

On California solar network data. The whole California data constitute a network. Thus, the major difference from using the Atlanta solar data is that x_t^k at each city k is defined to include spatial-temporal information from other Californian cities. In general, results on different Californian cities look very similar to each other so that we only provide plots on the Palo Alto solar data.

Figure 10 shows coverage/width versus $1 - \alpha$ line plots, whose results are similar to those in Figure 3. The only difference is that ARIMA now has higher coverage. Figure 11 shows similar boxplots as Figure 4. Lastly, we summarize the performance of traditional time-series methods and CP methods on time series from all Californian cities. Details are in Table 2 for the ridge regression. We only show results for ridge because results under different \mathcal{A} for CP methods are similar. We can see from the table that EnbPI performs similarly

as the time-series methods. On the other hand, the Winkler score⁵ by **EnbPI** using ridge regression can sometimes be the smallest so that it reaches a better balance between validity and efficiency. Meanwhile, ICP and WeightedICP can greatly lose coverage especially with multivariate X_t so that they should not be used for dynamic time-series data.

On the other hand, because **EnbPI** performs very similarly on the wind data, we will only apply it on the more challenging multi-step ahead inference with missing data.

B. Missing data, conditional coverage

On California solar network data: Figure 12(a) shows *conditional coverage* of **EnbPI** under RF at hours near noon, with the presence of missing data. The results look very similar to earlier ones, where conditional coverage by **EnbPI** is still validly attained.

On wind power data: Figure 12(b) shows conditional coverage of multi-step ahead inference of **EnbPI** under RF with missing data. No feature is available so we can only use past history of the wind power as response (that is, X_t is the history of Y_t). Note, one difference from applying **EnbPI** on earlier solar energy results is that we do not choose $s = 5$, but only train **EnbPI** on the whole 24 hourly data (for example, $s = 24$). We do so because this wind data do not exhibit clear differences at different hours of the day. Results show that **EnbPI** can reach valid conditional coverage at these hours, even under the presence of missing data.

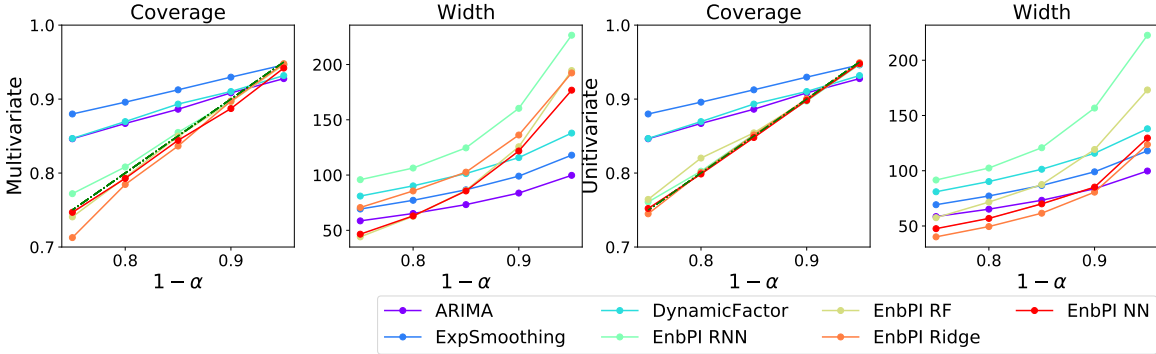


Figure 10: Solar power prediction in Palo Alto. Results are very similar as those in Figure 3, except an increase in ARIMA coverage.

B.4 Results on datasets in other domains

Data Description. We describe the additional three datasets being used, which are greenhouse gas emission data, air pollution data, and appliances energy data. The first dataset contains

5. Let the upper and lower end of the prediction interval at time t under level α be $L_t(\alpha)$, $U_t(\alpha)$, so width is $W_t(\alpha) = U_t(\alpha) - L_t(\alpha)$. Then, Winkler score (WS) is:

$$(WS)_t = \begin{cases} W_t(\alpha), & \text{if } L_t(\alpha) \leq y_t \leq U_t(\alpha) \\ W_t(\alpha) + 2 \cdot \frac{L_t(\alpha) - y_t}{\alpha}, & \text{if } y_t < L_t(\alpha) \\ W_t(\alpha) + 2 \cdot \frac{y_t - U_t(\alpha)}{\alpha}, & \text{if } y_t > U_t(\alpha) \end{cases}$$

It was used in Kath and Ziel (2021) as a quantitative measure of both coverage and width.

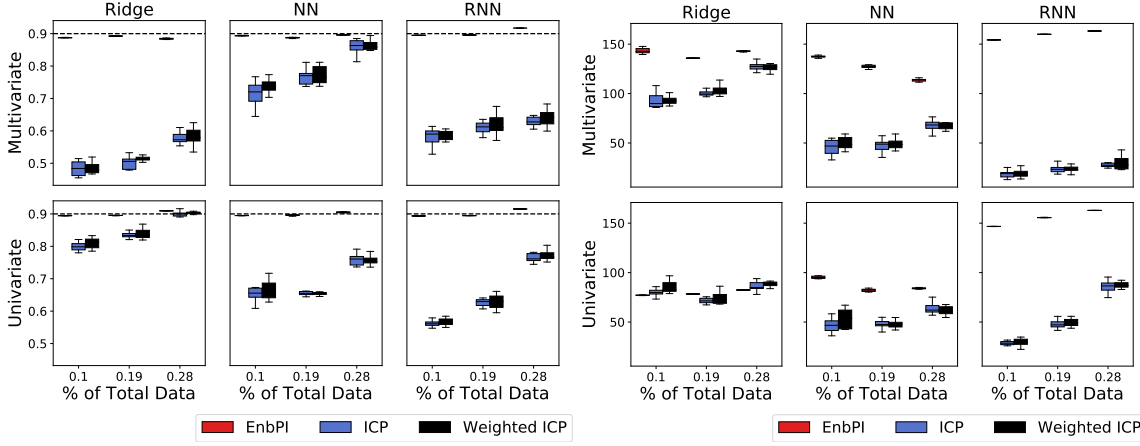
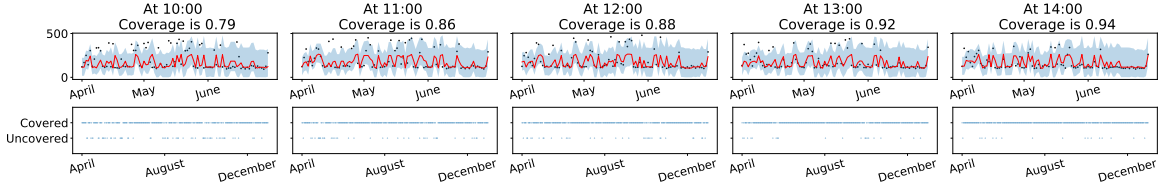
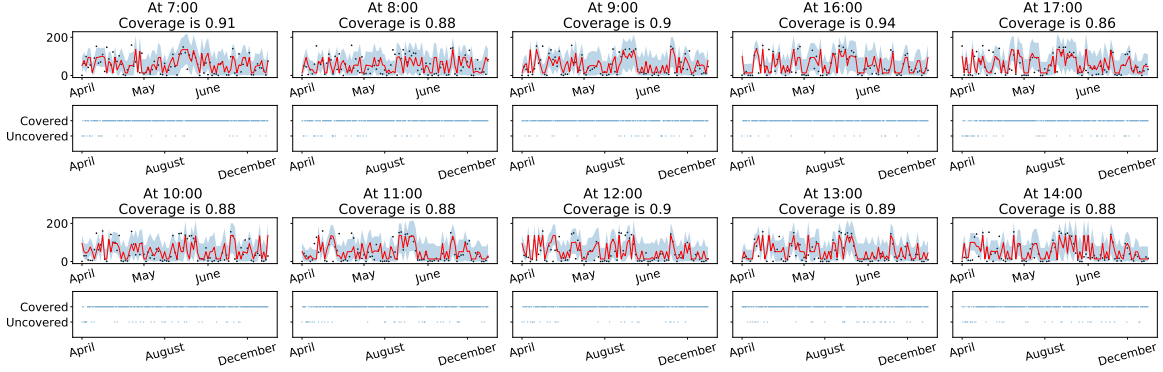


Figure 11: Solar power prediction in Palo Alto. Results are very similar as those in Figure 4



(a) Solar Palo Alto: **EnbPI** under RF with missing data



(b) Wind: **EnbPI** under RF with missing data, $s = 24$

Figure 12: Solar data in Palo Alto and wind data when **EnbPI** looks ahead beyond one step. Results are similar to those in Figure 5 (Solar Atlanta).

Greenhouse Gas observation (Greenhouse) (Lucas et al., 2015) from 5.10 till 7.31, 2010, with four samples every day and 6 hours apart between data points. The goal is to find the optimal weights for the 15 observation series to match the synthetic control series. The second dataset contains appliances energy usage (Appliances) (Candanedo et al., 2017). Consecutive data points are 10 minutes apart for about 4.5 months. We can use 27 different humidity and temperature indicators to predict the appliances' energy use in Wh. The third

Table 2: CP methods with Ridge. Coverage, width, and Winkler score on all 9 Californian cities. Smaller Winkler scores indicate a better balance between coverage and width. Bold cells indicate the smallest Winkler score for each city, where **EnbPI** using univariate X_t features consistently achieves the best balance.

Time series	Method	Multivariate			Univariate		
		Coverage	Width	Winkler Score	Coverage	Width	Winkler Score
Fremont	Ensemble	0.93	259.31	2.56e+06	0.95	135.64	1.43e+06
	ICP	0.67	142.40	6.76e+06	0.91	100.35	1.69e+06
	WeightedICP	0.69	150.68	5.21e+06	0.89	103.41	1.80e+06
	ARIMA	0.93	106.76	1.61e+06	0.93	107.32	1.61e+06
	ExpSmoothing	0.93	128.55	1.62e+06	0.94	124.93	1.60e+06
	DynamicFactor	0.94	148.87	1.73e+06	0.94	149.25	1.73e+06
Milpitas	Ensemble	0.93	257.14	2.53e+06	0.95	128.25	1.41e+06
	ICP	0.66	142.32	7.16e+06	0.91	100.49	1.63e+06
	WeightedICP	0.65	143.64	6.66e+06	0.91	101.13	1.69e+06
	ARIMA	0.92	99.71	1.70e+06	0.92	99.88	1.67e+06
	ExpSmoothing	0.94	126.03	1.62e+06	0.95	122.90	1.59e+06
	DynamicFactor	0.94	140.25	1.74e+06	0.94	140.51	1.74e+06
Mountain View	Ensemble	0.93	261.92	2.57e+06	0.95	126.76	1.41e+06
	ICP	0.64	140.73	7.41e+06	0.90	98.68	1.65e+06
	WeightedICP	0.66	154.15	6.23e+06	0.91	105.05	1.66e+06
	ARIMA	0.92	93.55	1.50e+06	0.92	94.76	1.48e+06
	ExpSmoothing	0.94	116.52	1.48e+06	0.94	116.84	1.48e+06
	DynamicFactor	0.94	133.90	1.62e+06	0.94	134.04	1.62e+06
North San Jose	Ensemble	0.93	261.04	2.55e+06	0.95	129.01	1.38e+06
	ICP	0.68	145.12	7.09e+06	0.90	103.55	1.65e+06
	WeightedICP	0.65	141.33	6.49e+06	0.90	100.84	1.69e+06
	ARIMA	0.92	101.12	1.60e+06	0.92	101.34	1.59e+06
	ExpSmoothing	0.94	120.17	1.54e+06	0.95	120.72	1.55e+06
	DynamicFactor	0.94	142.07	1.69e+06	0.94	142.32	1.69e+06
Palo Alto	Ensemble	0.92	258.10	2.54e+06	0.95	129.69	1.43e+06
	ICP	0.65	143.62	7.06e+06	0.90	100.40	1.66e+06
	WeightedICP	0.66	152.01	5.77e+06	0.91	106.87	1.66e+06
	ARIMA	0.93	99.33	1.51e+06	0.93	99.74	1.52e+06
	ExpSmoothing	0.94	119.96	1.52e+06	0.95	117.99	1.49e+06
	DynamicFactor	0.93	137.79	1.65e+06	0.93	137.98	1.65e+06
Redwood City	Ensemble	0.92	259.57	2.53e+06	0.95	132.31	1.43e+06
	ICP	0.68	151.59	6.44e+06	0.92	115.10	1.63e+06
	WeightedICP	0.64	149.69	6.47e+06	0.93	124.41	1.69e+06
	ARIMA	0.93	100.89	1.54e+06	0.93	101.72	1.54e+06
	ExpSmoothing	0.94	118.54	1.52e+06	0.94	118.49	1.52e+06
	DynamicFactor	0.94	142.87	1.64e+06	0.94	143.14	1.64e+06
San Mateo	Ensemble	0.93	257.20	2.50e+06	0.95	139.29	1.45e+06
	ICP	0.68	147.86	6.03e+06	0.92	127.50	1.77e+06
	WeightedICP	0.65	151.80	6.18e+06	0.93	126.55	1.72e+06
	ARIMA	0.92	105.25	1.63e+06	0.92	105.49	1.63e+06
	ExpSmoothing	0.94	128.21	1.59e+06	0.94	125.95	1.56e+06
	DynamicFactor	0.94	153.77	1.72e+06	0.94	154.09	1.72e+06
Santa Clara	Ensemble	0.93	251.93	2.47e+06	0.95	128.49	1.38e+06
	ICP	0.68	146.22	6.56e+06	0.91	105.98	1.64e+06
	WeightedICP	0.68	148.40	5.49e+06	0.92	110.49	1.66e+06
	ARIMA	0.93	101.71	1.55e+06	0.93	103.44	1.54e+06
	ExpSmoothing	0.94	117.94	1.53e+06	0.95	117.64	1.51e+06
	DynamicFactor	0.94	138.07	1.64e+06	0.94	138.31	1.64e+06
Sunnyvale	Ensemble	0.92	261.17	2.56e+06	0.95	131.52	1.42e+06
	ICP	0.68	153.19	6.73e+06	0.91	102.26	1.69e+06
	WeightedICP	0.63	150.14	6.77e+06	0.92	113.00	1.61e+06
	ARIMA	0.93	100.63	1.46e+06	0.93	98.32	1.47e+06
	ExpSmoothing	0.94	114.14	1.47e+06	0.94	114.69	1.44e+06
	DynamicFactor	0.94	137.63	1.59e+06	0.94	137.79	1.59e+06

dataset on Beijing air quality (Beijing air) (Zhang et al., 2017) contains air pollutants data from 12 nationally-controlled air-quality monitoring sites. The data is from 3.1, 2013 to 2.28, 2017. The goal is to predict PM2.5 air pollutant levels using 10 different air pollutants and meteorological variables. We use the data from the Tiantan district.

Results. We first show additional average coverage and width versus $1 - \alpha$ line plots as in Figure 3 (Solar power prediction in Atlanta). Then, we present grouped boxplots using both multivariate and univariate X_t as in Figure 4 (Solar power prediction in Atlanta). We do not examine conditional coverage on these dataset as we primarily aim to demonstrate the applicability of **EnbPI**.

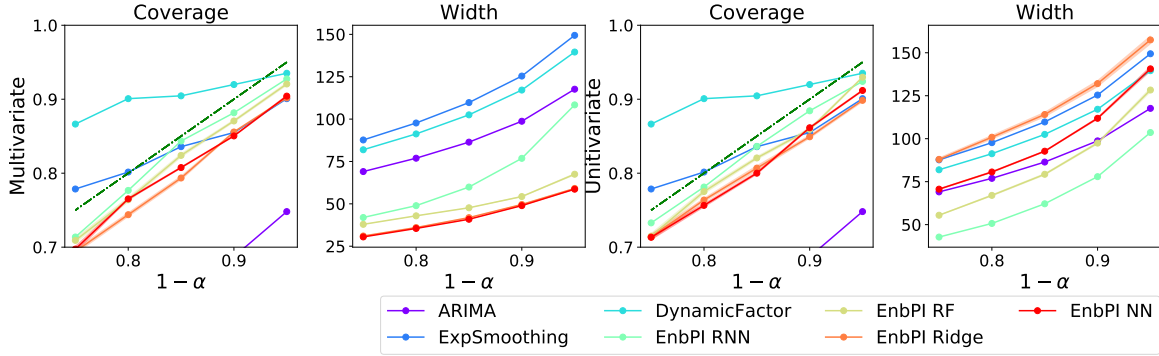
(1) *Observations from the other coverage/width versus $1 - \alpha$ plots*

- Figure 13 (a) (Greenhouse): Except the Dynamic Factor model, all methods tend to lose coverage; however, **EnbPI** under RNN tends to reach better coverage than other methods with much shorter interval widths. Therefore, we still favor **EnbPI**, although one needs to be more selective with the regression model \mathcal{A} .
- Figure 13 (b) (Appliances Energy): All time-series methods no longer lose coverage, but **EnbPI** under RNN yields shortest intervals without coverage losses when X_t is multivariate. When X_t is univariate, **EnbPI** almost always maintains coverage and yields much shorter intervals than time-series methods.
- Figure 13 (c) (Beijing Air): Time-series methods do not lose coverage. However, **EnbPI** under NN, RF, or Ridge with univariate X_t can produce shorter intervals with exact coverage guarantee.

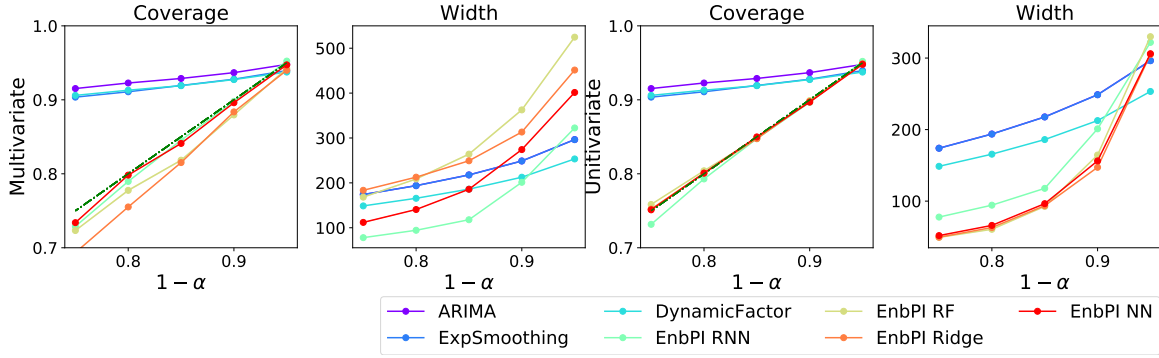
(2) *Observations from the other grouped boxplots*

- Figure 14 (a) (Greenhouse): **EnbPI** almost never loses coverage, whereas ICP and WeightedICP can significantly under-cover (for example, see NN on univariate X_t). Moreover, **EnbPI** coverage and widths have much less variance than the other ones.
- Figure 14 (b) (Appliances Energy) reveals similar patterns. In particular, ICP and WeightedICP can significantly lose coverage significantly (for example, see ridge on multivariate X_t). Moreover, ICP and WeightedICP also have higher widths with much larger variances than **EnbPI** (for example, see RNN on multivariate X_t). Overall, we notice that intervals on univariate versions are much shorter than those on multivariate versions, likely because the past history of energy use is more predictive of future energy use than the exogenous variables such as humidity and temperature of the surrounding (for example, kitchen, bathroom, living room, etc.).
- Figure 14 (c) (Beijing Air) shows similar performances by all three CP methods, although ICP and Weighted ICP may greatly lose coverage (for example, see ridge on multivariate X_t).

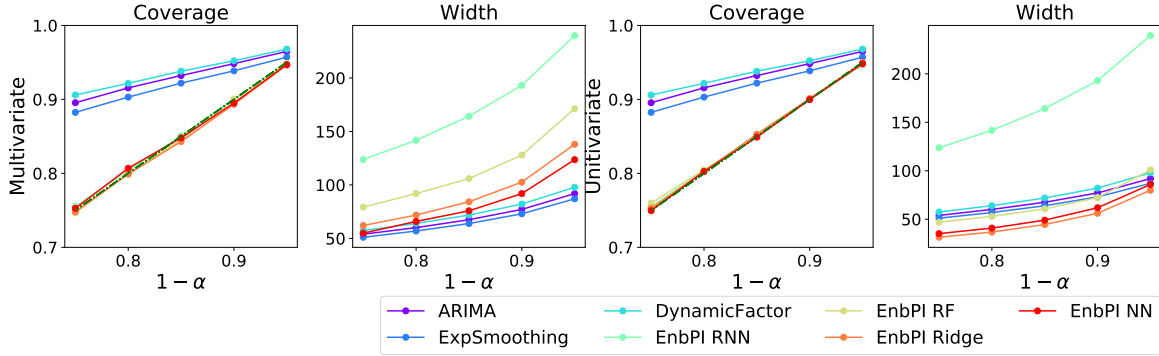
In general, we think **EnbPI** is stable across different combinations of prediction algorithms and datasets. Since other CP methods such as ICP and WeightedICP can severely lose coverage, we advocate the use of **EnbPI** for time-series predictive inference. Regarding interval width, using the history of the response (univariate version) to predict its future values tends to yield shorter intervals.



(a) Greenhouse Gas

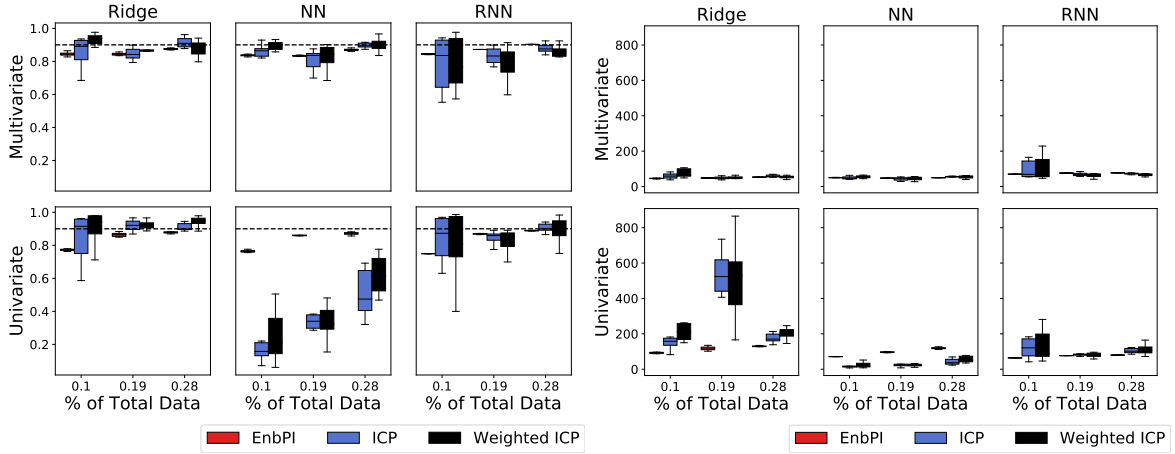


(b) Appliances Energy

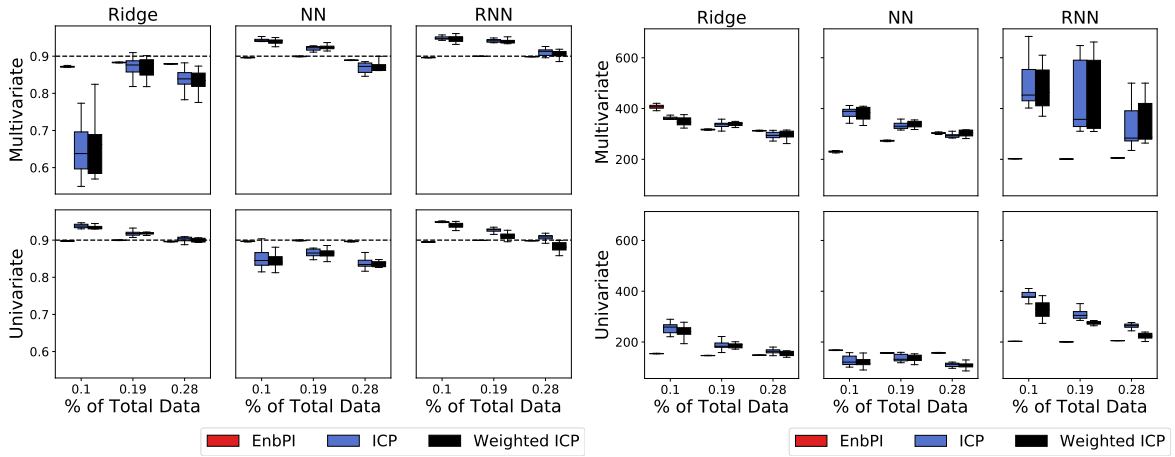


(c) Beijing Air

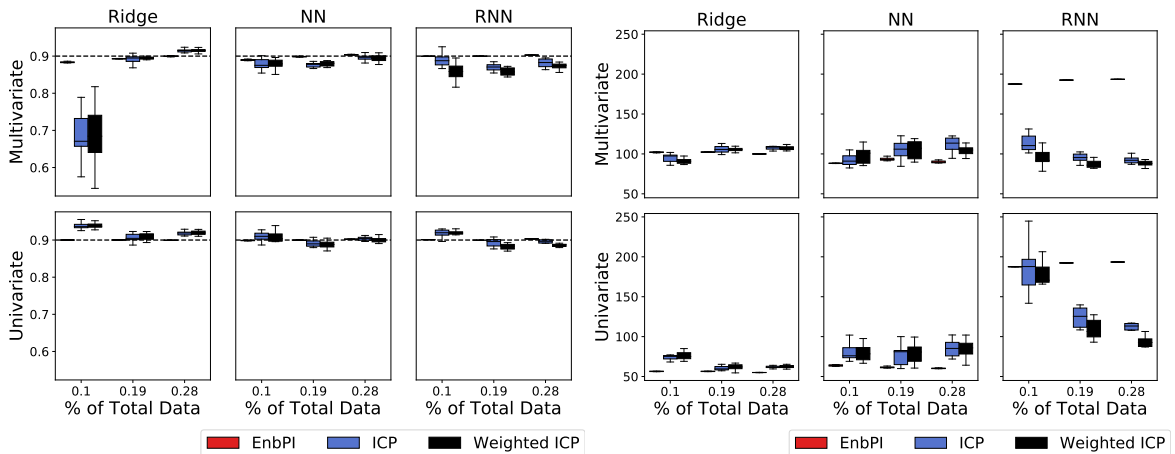
Figure 13: Prediction on three other time series. Average coverage and width versus $1 - \alpha$ target coverage by **EnbPI** under different prediction algorithms and by ARIMA, Exponential Smoothing, and Dynamic Factor models. Five equally spaced $1 - \alpha \in [0.75, 0.95]$ are chosen. The green dash-dotted line at 0.9 represents the target coverage.



(a) Greenhouse Gas



(b) Appliances Energy Gas



(c) Beijing Air

Figure 14: Prediction on three other time series. Boxplots of average coverage (top) and width (bottom) by EnbPI, ICP, and WeightedICP, whose training data vary as a percentage of total data (x-axis). Each box contains results from 10 independent trials. The black dash dotted line at 0.9 indicates target coverage.

B.5 Anomaly detection setup

Data Description. The data come from the same source as those in (Xu and Xie, 2021), but sensors are chosen differently, and some competing methods are also different. Thus, we follow how Xu and Xie (2021) define anomalies with minor differences; the definitions are emphasized here for self-contained exposition. Suppose K sensors are in the network and T observations are available at each sensor. Denote Y_{tk} as the traffic flow observation of sensor k at time t . The symbol $\mathbf{Y} = [Y_{tk}]$ denotes the whole data matrix with no missing entries. Then for each $k \in \{1, \dots, 10\}$ and $t \in \{1, \dots, 17520\}$ (48×365 bi-hourly data in 2020), define Y_{tk} as an anomaly if

$$Y_{tk} \geq q_{1-\alpha}(Y_{t,N_k}^{-d}) \text{ or } Y_{tk} \leq q_{\alpha}(Y_{t,N_k}^{-d}),$$

where $q_{\alpha}(\cdot)$ is the α percentile of its input vector, N_k contains sensors closest to k (including itself), and Y_{t,N_k}^{-d} contains past d hourly flows from sensors in N_k . Let $\alpha = 0.01$, $d = |N_k| = 5$, all of which are unknown.

We remark that the training data in \mathbf{Y} is given to us with 30% missing entries in each sensor column. Thus, we use the `IterativeImputer` from the Python `sklearn` package to denote the imputed matrix. Denote $\hat{\mathbf{Y}}$ as the imputed data matrix. To apply `EnbPI`, we first define $X_{tk} := \hat{Y}_{t,\hat{N}_k}^{-m} \in \mathbb{R}^{m|\hat{N}_k|}$ as the past m hourly flows from \hat{N}_k closest sensors to k . Let $m = |\hat{N}_k| = 8$. Then, the test data Y_{tk} is predicted as an anomaly if its residual is either higher than $1 - \alpha + \hat{\beta}$ or lower than $\hat{\beta}$ quantile of residuals on Y_{t,\hat{N}_k}^{-m} .

Four unsupervised methods. All the unsupervised methods are implemented in the `pyod` library in Python. We consider `IForest`, `PCA`, `OCSVM`, and `HBOS` and descriptions below mostly come from the package description with minor changes:

- The `IsolationForest` (`IForest`) “isolates” observations x_t by randomly selecting a feature of x_t and then randomly selecting a split value between the maximum and minimum values of the selected feature. See Liu et al. (2012).
- In the `Principal Component Analysis` (`PCA`) for anomaly detection, covariance matrix of the data is first decomposed to orthogonal vectors, which are eigenvectors. Then, outlier scores are obtained as the sum of the projected distance of a sample on all eigenvectors. See Aggarwal (2015).
- The one-class support vector machine (`OCSVM`) is a wrapper of `scikit-learn` one-class SVM Class with more functionalities. See <https://scikit-learn.org/stable/modules/svm.html#svm-outlier-detection> for detailed descriptions.
- The `Histogram-based Outlier Detection` (`HBOS`) assumes feature independence in x_t and calculates the degree of outlyingness by building histograms. See Goldstein and Dengel (2012).

Four supervised methods. All the supervised methods are taken as binary classification methods from the `sklearn` package in Python. We take descriptions of methods from the package and specify the following parameters for each method

- The `Gradient Boosting Classifier` (`GBoosting`) builds an additive model in a forward stage-wise fashion; it allows for the optimization of arbitrary differentiable loss functions. We build 100 estimators, pick a learning rate of 1, and let maximum depth be 1.

- The Multi-layer Perceptron classifier (MLPClassifier) optimizes the log-loss function. We use LBFGS for optimization, let l_2 penalty α be 1e-5, and pick two hidden layers with 5 neurons in the first and 2 in the second.
- The k -nearest neighbor (KNN) algorithm is specified with $k = 20$ and weights=“distance”, so that closer neighbors of a query point will have a greater influence than neighbors which are further away.
- The support vector classification (SVC) uses all the default settings except with gamma=“auto”, which uses $1 / \#$ features as the kernel coefficient.

References

- Charu C Aggarwal. Outlier analysis. In *Data mining*, pages 237–263. Springer, 2015.
- Samaneh Aminikhanghahi and Diane J Cook. A survey of methods for time series change point detection. *Knowledge and information systems*, 51(2):339–367, 2017.
- A. Angelopoulos, Stephen Bates, J. Malik, and Michael I. Jordan. Uncertainty sets for image classifiers using conformal prediction. *ArXiv*, abs/2009.14193, 2020.
- Krishna B. Athreya and Sastry G. Pantula. A note on strong mixing of arma processes. *Statistics and Probability Letters*, 4(4):187–190, 1986. ISSN 0167-7152. doi: [https://doi.org/10.1016/0167-7152\(86\)90064-7](https://doi.org/10.1016/0167-7152(86)90064-7). URL <https://www.sciencedirect.com/science/article/pii/0167715286900647>.
- Marta Bańbura and Michele Modugno. Maximum likelihood estimation of factor models on datasets with arbitrary pattern of missing data. *Journal of Applied Econometrics*, 29(1):133–160, 2014.
- Rina Foygel Barber, Emmanuel J Candes, Aaditya Ramdas, and Ryan J Tibshirani. The limits of distribution-free conditional predictive inference. *arXiv preprint arXiv:1903.04684*, 2019a.
- Rina Foygel Barber, Emmanuel J. Candes, Aaditya Ramdas, and Ryan J. Tibshirani. Predictive inference with the jackknife+, 2019b.
- Stephen Bates, Emmanuel Candès, Lihua Lei, Yaniv Romano, and Matteo Sesia. Testing for outliers with conformal p-values, 2021.
- Peter J Bickel, Ya’acov Ritov, Alexandre B Tsybakov, et al. Simultaneous analysis of lasso and dantzig selector. *The Annals of statistics*, 37(4):1705–1732, 2009.
- Leo Breiman. Bagging predictors. *Machine learning*, 24(2):123–140, 1996.
- Leo Breiman. Random forests. *Machine learning*, 45(1):5–32, 2001.
- Peter J Brockwell, Richard A Davis, and Stephen E Fienberg. Time series: theory and methods: theory and methods. *Springer Science & Business Media*, 1991.

- Luis M Candanedo, Véronique Feldheim, and Dominique Deramaix. Data driven prediction models of energy use of appliances in a low-energy house. *Energy and buildings*, 140:81–97, 2017.
- Maxime Cauchois, Suyash Gupta, Alnur Ali, and John C. Duchi. Robust validation: Confident predictions even when distributions shift, 2020.
- Shiyun Chen and Shiva Kasiviswanathan. Contextual online false discovery rate control. In *Proceedings of the Twenty Third International Conference on Artificial Intelligence and Statistics*, volume 108 of *Proceedings of Machine Learning Research*, pages 952–961, Online, 26–28 Aug 2020. PMLR. URL <http://proceedings.mlr.press/v108/chen20b.html>.
- Xiaohong Chen and Halbert White. Improved rates and asymptotic normality for non-parametric neural network estimators. *IEEE Transactions on Information Theory*, 45(2): 682–691, 1999.
- Victor Chernozhukov, Kaspar Wüthrich, and Zhu Yinchu. Exact and robust conformal inference methods for predictive machine learning with dependent data. volume 75 of *Proceedings of Machine Learning Research*, pages 732–749. PMLR, 06–09 Jul 2018. URL <http://proceedings.mlr.press/v75/chernozhukov18a.html>.
- Victor Chernozhukov, Kaspar Wuthrich, and Yinchu Zhu. An exact and robust conformal inference method for counterfactual and synthetic controls. *arXiv preprint arXiv:1712.09089*, 2020.
- Jaquelin Cochran, Paul Denholm, Bethany Speer, and Mackay Miller. Grid integration and the carrying capacity of the us grid to incorporate variable renewable energy. Technical report, National Renewable Energy Lab.(NREL), Golden, CO (United States), 2015.
- Francisco Díaz-González, Andreas Sumper, Oriol Gomis-Bellmunt, and Roberto Villafila-Robles. A review of energy storage technologies for wind power applications. *Renewable and sustainable energy reviews*, 16(4):2154–2171, 2012.
- Yadolah Dodge. *The Oxford dictionary of statistical terms*. Oxford University Press on Demand, 2006.
- Robin Dunn, Larry Wasserman, and Aaditya Ramdas. Distribution-free prediction sets with random effects, 2020.
- James Durbin and Siem Jan Koopman. *Time series analysis by state space methods*. Oxford university press, 2012.
- Adam Fisch, Tal Schuster, Tommi Jaakkola, and Dr.Regina Barzilay. Few-shot conformal prediction with auxiliary tasks. In Marina Meila and Tong Zhang, editors, *Proceedings of the 38th International Conference on Machine Learning*, volume 139 of *Proceedings of Machine Learning Research*, pages 3329–3339. PMLR, 18–24 Jul 2021a. URL <https://proceedings.mlr.press/v139/fisch21a.html>.

- Adam Fisch, Tal Schuster, Tommi S. Jaakkola, and Regina Barzilay. Efficient conformal prediction via cascaded inference with expanded admission. In *International Conference on Learning Representations*, 2021b. URL <https://openreview.net/forum?id=tnSo6VRLmT>.
- Isaac Gibbs and Emmanuel J. Candès. Adaptive conformal inference under distribution shift. 2021.
- Markus Goldstein and Andreas Dengel. Histogram-based outlier score (hbos): A fast unsupervised anomaly detection algorithm. *KI-2012: Poster and Demo Track*, pages 59–63, 2012.
- Chirag Gupta, Arun K Kuchibhotla, and Aaditya K Ramdas. Nested conformal prediction and quantile out-of-bag ensemble methods. *arXiv preprint arXiv:1910.10562*, 2019.
- Chirag Gupta, Aleksandr Podkopaev, and Aaditya Ramdas. Distribution-free binary classification: prediction sets, confidence intervals and calibration, 2021.
- C.H. Hesse. Rates of convergence for the empirical distribution function and the empirical characteristic function of a broad class of linear processes. *Journal of Multivariate Analysis*, 35(2):186 – 202, 1990. ISSN 0047-259X. doi: [https://doi.org/10.1016/0047-259X\(90\)90024-C](https://doi.org/10.1016/0047-259X(90)90024-C). URL <http://www.sciencedirect.com/science/article/pii/0047259X9090024C>.
- Rob Hyndman, Anne B Koehler, J Keith Ord, and Ralph D Snyder. *Forecasting with exponential smoothing: the state space approach*. Springer Science & Business Media, 2008.
- Rafael Izbicki, Gilson Shimizu, and Rafael Stern. Flexible distribution-free conditional predictive bands using density estimators. volume 108 of *Proceedings of Machine Learning Research*, pages 3068–3077, Online, 26–28 Aug 2020. PMLR. URL <http://proceedings.mlr.press/v108/izbicki20a.html>.
- Christopher Kath and Florian Ziel. Conformal prediction interval estimation and applications to day-ahead and intraday power markets. *International Journal of Forecasting*, 37(2):777–799, Apr 2021. ISSN 0169-2070. doi: 10.1016/j.ijforecast.2020.09.006. URL <http://dx.doi.org/10.1016/j.ijforecast.2020.09.006>.
- Byol Kim, Chen Xu, and Rina Foygel Barber. Predictive inference is free with the jackknife+-after-bootstrap, 2020.
- Danijel Kivaranovic, Kory D. Johnson, and Hannes Leeb. Adaptive, distribution-free prediction intervals for deep networks. volume 108 of *Proceedings of Machine Learning Research*, pages 4346–4356, Online, 26–28 Aug 2020. PMLR. URL <http://proceedings.mlr.press/v108/kivaranovic20a.html>.
- Michael R Kosorok. *Introduction to empirical processes and semiparametric inference*. Springer Science & Business Media, 2007.
- Jens-Peter Kreiss and E. Paparoditis. Bootstrap methods for dependent data: A review. *Journal of The Korean Statistical Society*, 40:357–378, 2011.

- Stéphane Lathuilière, Pablo Mesejo, Xavier Alameda-Pineda, and Radu Horaud. A comprehensive analysis of deep regression. *IEEE transactions on pattern analysis and machine intelligence*, 2019.
- Fei Tony Liu, Kai Ming Ting, and Zhi-Hua Zhou. Isolation-based anomaly detection. *ACM Transactions on Knowledge Discovery from Data (TKDD)*, 6(1):1–39, 2012.
- DD Lucas, C Yver Kwok, P Cameron-Smith, H Graven, D Bergmann, TP Guilderson, R Weiss, and R Keeling. Designing optimal greenhouse gas observing networks that consider performance and cost. *Geoscientific Instrumentation, Methods and Data Systems*, 4(1):121, 2015.
- H. Papadopoulos, V. Vovk, and A. Gammerman. Conformal prediction with neural networks. In *19th IEEE International Conference on Tools with Artificial Intelligence (ICTAI 2007)*, volume 2, pages 388–395, 2007.
- Aaditya Ramdas, Fanny Yang, Martin J Wainwright, and Michael I Jordan. On-line control of the false discovery rate with decaying memory. In *Advances in Neural Information Processing Systems*, volume 30, pages 5650–5659. Curran Associates, Inc., 2017. URL <https://proceedings.neurips.cc/paper/2017/file/7f018eb7b301a66658931cb8a93fd6e8-Paper.pdf>.
- Emmanuel Rio. *Asymptotic theory of weakly dependent random processes*, volume 80. Springer, 2017.
- Yaniv Romano, Evan Patterson, and Emmanuel Candes. Conformalized quantile regression. In *Advances in Neural Information Processing Systems*, pages 3543–3553, 2019.
- Yaniv Romano, M. Sesia, and E. Candès. Classification with valid and adaptive coverage. *arXiv: Methodology*, 2020.
- Murray Rosenblatt. A central limit theorem and a strong mixing condition. *Proceedings of the National Academy of Sciences of the United States of America*, 42 1:43–7, 1956.
- Glenn Shafer and Vladimir Vovk. A tutorial on conformal prediction. *Journal of Machine Learning Research*, 9(Mar):371–421, 2008.
- Ryan J Tibshirani, Rina Foygel Barber, Emmanuel Candes, and Aaditya Ramdas. Conformal prediction under covariate shift. In *Advances in Neural Information Processing Systems*, pages 2530–2540, 2019.
- Denis Volkhonskiy, Evgeny Burnaev, Ilia Nouretdinov, Alexander Gammerman, and Vladimir Vovk. Inductive conformal martingales for change-point detection. In *Conformal and Probabilistic Prediction and Applications*, pages 132–153. PMLR, 2017.
- Vladimir Vovk. Testing randomness online. *Statistical Science*, October 2020. ISSN 0883-4237. To appear.
- Vladimir Vovk. Conformal testing in a binary model situation, 2021.

- Vladimir Vovk, Ivan Petej, Ilia Nouretdinov, Ernst Ahlberg, Lars Carlsson, and Alex Gammernan. Retrain or not retrain: Conformal test martingales for change-point detection, 2021.
- David H Wolpert and William G Macready. No free lunch theorems for optimization. *IEEE transactions on evolutionary computation*, 1(1):67–82, 1997.
- Liyan Xie, Shaofeng Zou, Yao Xie, and Venugopal V Veeravalli. Sequential (quickest) change detection: Classical results and new directions. *IEEE Journal on Selected Areas in Information Theory*, 2(2):494–514, 2021.
- Chen Xu and Yao Xie. Conformal anomaly detection on spatio-temporal observations with missing data, 2021.
- Gianluca Zeni, Matteo Fontana, and Simone Vantini. Conformal prediction: a unified review of theory and new challenges. *arXiv preprint arXiv:2005.07972*, 2020.
- Shuyi Zhang, Bin Guo, Anlan Dong, Jing He, Ziping Xu, and Song Xi Chen. Cautionary tales on air-quality improvement in beijing. *Proceedings of the Royal Society A: Mathematical, Physical and Engineering Sciences*, 473(2205):20170457, 2017.